

# LandSegmenter: Towards a Flexible Foundation Model for Land Use and Land Cover Mapping

Chenyang Liu<sup>a,b</sup>, Wei Huang<sup>a</sup> and Xiao Xiang Zhu<sup>a,b,\*</sup>

<sup>a</sup>Chair of Data Science in Earth Observation, Technical University of Munich, Munich, 80333, Germany

<sup>b</sup>Munich Center for Machine Learning (MCML), Munich, 80333, Germany

## ARTICLE INFO

### Keywords:

remote sensing  
land use and land cover mapping  
semantic segmentation  
weakly supervised learning  
noisy labels  
zero-shot

## ABSTRACT

Land Use and Land Cover (LULC) mapping is a fundamental task in Earth Observation (EO). However, current LULC models are typically developed for a specific modality and a fixed class taxonomy, limiting their generability and broader applicability. Recent advances in foundation models (FMs) offer promising opportunities for building universal models. Yet, task-agnostic FMs often require fine-tuning for downstream applications, whereas task-specific FMs rely on massive amounts of labeled data for training, which is costly and impractical in the remote sensing (RS) domain. To address these challenges, we propose LandSegmenter, an LULC FM framework that resolves three-stage challenges at the input, model, and output levels. From the input side, to alleviate the heavy demand on labeled data for FM training, we introduce LAnd Segment (LAS), a large-scale, multi-modal, multi-source dataset built primarily with globally sampled weak labels from existing LULC products. LAS provides a scalable, cost-effective alternative to manual annotation, enabling large-scale FM training across diverse LULC domains. For model architecture, LandSegmenter integrates an RS-specific adapter for cross-modal feature extraction and a text encoder for semantic awareness enhancement. At the output stage, we introduce a class-wise confidence-guided fusion strategy to mitigate semantic omissions and further improve LandSegmenter's zero-shot performance. We evaluate LandSegmenter on six precisely annotated LULC datasets spanning diverse modalities and class taxonomies. Extensive transfer learning and zero-shot experiments demonstrate that LandSegmenter achieves competitive or superior performance, particularly in zero-shot settings when transferred to unseen datasets. These results highlight the efficacy of our proposed framework and the utility of weak supervision for building task-specific FMs. The code and dataset are publicly available at <https://github.com/zhu-xlab/LandSegmenter.git>.

## 1. Introduction

Land Use and Land Cover (LULC) mapping is critical for many real Earth Observation (EO) applications (Chen et al., 2025; Wang et al., 2023b; Shi et al., 2025). Joint efforts from Remote Sensing (RS) and Computer Vision (CV) communities have driven significant advances in LULC mapping using traditional handcrafted and modern deep-learning-based approaches (Zhu et al., 2017; He et al., 2018; Prudente et al., 2022). However, these models are often tailored to specific geographic regions, data types, and tasks, constraining generalizability and scalability for large-scale deployment (Chen and Bruzzone, 2023).

Recent developments in Foundation Models (FMs) offer a promising avenue for addressing these limitations. Task-agnostic FMs leverage Self-Supervised Learning (SSL) (He et al., 2020, 2022; Caron et al., 2021) to enhance feature representation from unlabeled data, enabling efficient adaptation to downstream tasks with minimal labeled data (Wang et al., 2022b). Conversely, task-specific FMs utilize extensive labeled data to achieve robust performance for specialized purposes, exemplified by the Segment Anything Model (SAM) series (Kirillov et al., 2023; Ravi et al., 2024) for promptable segmentation. These advancements suggest the potential of FMs to provide unified and scalable solutions.

However, applying SAM to LULC mapping presents several challenges due to unique RS data characteristics, including diverse modalities, varying spatial resolutions, and domain-specific features. SAM models were trained on high-resolution RGB natural images and videos. They struggle with multispectral RS data, which are often of medium to low spatial resolution, such as Sentinel (10m) and Landsat (30m). While SAM performs well on instance segmentation of discrete, well-bounded objects (e.g., cars), it falls short when handling region-level classes (e.g., grass) that represent continuous or less distinctly bounded land surfaces (Ji et al., 2024; Zhu et al., 2025) and are essential for accurate LULC mapping. Its reliance on geometric prompts (e.g., points, boxes) also limits its effectiveness in dense mapping.

On the other hand, training task-specific FMs demands extensive labeled data. Precise labels are costly and labor-intensive. For instance, SAM training relies on millions of images and over a billion annotated masks (Kirillov et al., 2023), a scale impractical for RS applications. Weakly supervised pretraining offers a solution by utilizing abundant albeit imperfect labels (Mahajan et al., 2018; Ghadiyaram et al., 2019; Jia et al., 2021). While some studies (Maggiore et al., 2017; Liu et al., 2025) have explored pixel-wise weak labels for pretraining, they primarily focus on simpler or smaller-scale tasks. Its potential in complex, large-scale dense prediction tasks remains underexplored. LULC mapping, with widely available noisy products easily paired with RS imagery, offers an ideal test case. Although

\*Corresponding author

✉ [chenyang.liu@tum.de](mailto:chenyang.liu@tum.de) (C. Liu); [w2wei.huang@tum.de](mailto:w2wei.huang@tum.de) (W. Huang);  
[xiaoxiang.zhu@tum.de](mailto:xiaoxiang.zhu@tum.de) (X.X. Zhu)  
ORCID(s):

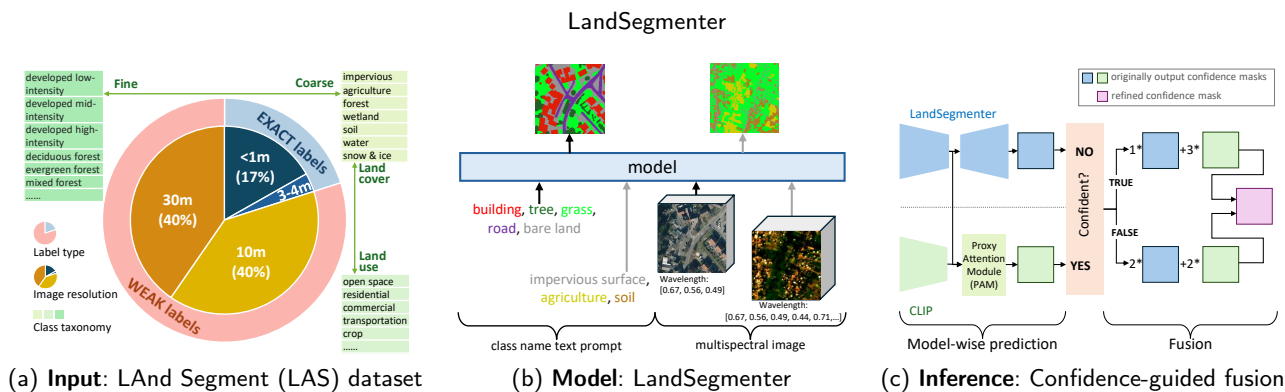


**Fig. 1:** Overview of the proposed workflow for LULC FM construction, comprising three main stages. (a) LAS dataset curation: a globally sampled collection of RS imagery spanning diverse modalities and LULC categories, primarily weakly labeled at low cost. (b) LandSegementer model design: a task-adaptive architecture capable of processing varying multispectral inputs and producing LULC maps tailored to user-defined category sets. (c) Zero-shot inference enhancement: a confidence-guided fusion strategy to improve recognition of semantically omitted or underrepresented classes during inference.

these products contain label noise from automatic errors, ambiguities, and temporal inconsistencies, they can provide sufficient supervision for models to capture dominant spatial patterns while remaining fairly robust to noise.

In this work, we introduce LandSegementer, a task-specific FM for LULC mapping, with the goals of: 1) enhancing model flexibility in both input modalities and output categories; and 2) equipping the model with zero-shot capabilities while maintaining its fine-tuning potential. To this end, we build a workflow at three stages as in Fig. 1.

First, at the **input** stage, we curate the **LAnd Segment (LAS) dataset**, which leverages existing LULC products as weak supervision to address the scarcity of medium-to-low resolution annotations for model training. As illustrated in Fig. 1 (a), the exact-to-weak label ratio of LAS is 1:4. It reflects real-world scenarios, in which high-quality annotations are typically limited to high-resolution RS imagery, whereas LULC products are predominantly of medium-to-low resolution. LAS also employs more region-level classes to enrich the semantic understanding of Earth surface structures. Through extensive experiments, we demonstrate the effectiveness of weak labels to train segmentation FMs.

Then, to enhance the **model's** adaptability for LULC mapping, we design **LandSegementer** by integrating task-adaptive feature extraction modules with a dynamic fusion strategy. We adopt SAM2's backbone for its robust hierarchical multi-scale spatial feature extraction capability, complemented with multispectral features from DOFA (Xiong et al., 2024) and detail-enhanced representations from high-frequency components. The additional inputs are aligned with the main feature stream through the Attention-based Fusion Module (AFM) at intermediate layers. Additionally, we replace SAM2's geometric prompter with the text encoder from GeoRSClip (Zhang et al., 2024b) to boost LandSegementer's semantic understanding for flexible and concept-aware output generation. The integration of the text prompter endows LandSegementer with the zero-shot segmentation capability, which benefits LULC mapping in both training and inference stages. During training, using class names as prompts enables the simultaneous use of multiple

heterogeneous datasets. This allows the model to leverage complementary information to improve performance and generalization across various sensors, regions, and spatial resolutions. At inference, users can flexibly generate customized maps under diverse classification needs with a single model, which effectively reduces the effort required to harmonize existing products. In this way, LandSegementer inherits strong generalization ability from existing FMs while gaining explicit semantic understanding for LULC mapping.

Finally, to enhance zero-shot **inference**, we introduce a **confidence-guided fusion** strategy to handle semantic omissions. This mechanism uses class-wise confidence scores to guide the fusion of predictions from LandSegementer and CLIP-style models, thereby improving performance on unseen classes of LandSegementer. These omitted classes are often object-level entities (e.g., cars) that are absent from standard LULC labels but well recognized by CLIP models.

We assess LandSegementer's transferability on six precisely annotated LULC datasets across different modalities and categories. Results show that LandSegementer effectively leverages weak supervision to achieve a balance between scalability and precision. We believe our approach offers valuable insights for future research where accurate annotations are scarce but large-scale noisy labels are accessible. The main contributions are summarized as follows:

- We propose the first LULC FM termed LandSegementer, which offers high flexibility in both input and output ends. The model supports zero-shot inference and can also be fine-tuned in downstream tasks.
- We design a three-stage workflow for constructing LandSegementer, emphasizing the effective use of large-scale weak supervision to enable scalable FM training, and introducing a class-wise confidence-guided fusion strategy to enhance zero-shot inference.
- We conduct extensive evaluations across six benchmark LULC datasets with precise annotations. The experimental results demonstrate the effectiveness and generalizability of LandSegementer under diverse imaging conditions and label granularities.

Next, we review related work in Sec. 2, describe the LULC FM construction workflow in Sec. 3–Sec. 5, present experimental results in Sec. 6, and conclude in Sec. 7.

## 2. Related Work

We briefly review recent progress on FMs, weakly supervised pretraining, and zero-shot semantic segmentation.

### 2.1. Foundation models

SSL plays a crucial role in developing task-agnostic FMs from vast unlabeled data (Zhu et al., 2024; Zhao et al., 2024). Prominent SSL methods include generative Masked Autoencoders (MAE) (He et al., 2022) and contrastive techniques (Caron et al., 2021; Chen et al., 2020). In EO, SSL is tailored to unique characteristics of RS imagery, such as RingMo’s patch-incomplete Masked Image Modeling (MIM) (Sun et al., 2023), SatMAE’s temporal-spectral embeddings for multispectral data (Cong et al., 2022; Norman et al., 2024), and Scale-MAE’s scale-aware pretraining (Reed et al., 2023). Recently, multi-modal SSL has further advanced cross-modal representation learning (Wang et al., 2025; Guo et al., 2023; Fuller et al., 2023; Astruc et al., 2024). Among them, SkySense++ (Wu et al., 2025) focuses on multimodal representation learning across optical and SAR imagery via a semantic-enhanced pretraining strategy. DOFA (Xiong et al., 2024) leverages hypernetworks to generate dynamic patch embedding weights from wavelength, enabling high adaptability across diverse inputs. While reducing reliance on labeled data, they often require task-specific fine-tuning. The SAM models (Kirillov et al., 2023; Ravi et al., 2024), pretrained on millions of natural images or videos and billions of masks, offer a breakthrough as the first segmentation FMs (Li et al., 2025a; Zhou et al., 2024b; Song et al., 2021; Shankar et al., 2023). SAM is specific to spatial understanding yet inherently semantic-unaware. Common approaches generate geometric prompts from semantic cues (Chen et al., 2024a; Wang et al., 2024a) or classify SAM’s segments (Zhang et al., 2024a; Wang et al., 2024c), lacking flexibility and convenience. Besides, SAM is less capable of coping with RS images of diverse modalities and scales due to a lack of relevant training data.

### 2.2. Weakly supervised pretraining

The success of SAM relies heavily on vast labeled data. As a cost-efficient alternative, researchers are exploring “weak” labels—scalable and affordable, albeit noisy—for model training (Singh et al., 2022). Studies have shown that deep learning models can tolerate some label noise (Zhang et al., 2021; Liu et al., 2024a). The models pretrained with noisy labels maintain strong feature learning and transferability across tasks like image classification (Mahajan et al., 2018), video analysis (Ghadiyaram et al., 2019), and image-text alignment (Jia et al., 2021). Several works (Kaiser et al., 2017; Maggiori et al., 2017; Liu et al., 2025) have explored using pixel-wise weak labels in traditional pretraining paradigms, revealing that shallower layers (closer to the input, typically corresponding to encoders) are less affected by

label noise and remain robust after fine-tuning. For instance, CromSS (Liu et al., 2025) leverages modality-specific encoders within middle and late fusion frameworks during the noisy label pretraining stage, while transferring only the encoders to downstream tasks. In contrast, our work extends the benefits of noisy label pretraining to enhance semantic understanding for zero-shot segmentation. Moreover, unlike CromSS, which relies on separate backbones for different modalities, our model improves multimodal flexibility by handling diverse inputs within a unified framework.

### 2.3. Zero-shot semantic segmentation

Contrastive Language-Image Pretraining (CLIP) models (Radford et al., 2021) have advanced zero-shot semantic segmentation, also known as Open-Vocabulary Semantic Segmentation (OVSS), by aligning image and text features to overcome the limitations of closed-set settings (Zhou et al., 2024a). However, CLIP is trained at the image level and often struggles to depict details in dense prediction tasks. To alleviate this issue, MaskCLIP leverages value embeddings from CLIP’s final layer to improve localization (Zhou et al., 2022). Others employ self-self attention mechanisms (e.g. value-value (Li et al., 2025b), query-query, key-key, or their combinations (Lan et al., 2024a; Wang et al., 2024b)) to denoise attention maps. Vision Foundation Model (VFM) features have also been integrated to improve CLIP’s spatial awareness, either in a training-free (Lan et al., 2024b) or training (Shan et al., 2024) way. Still, CLIP-based models show reduced sensitivity to RS images. SegEarth-OV addresses this by introducing a fine-tuned upsampler to recover spatial details (Li et al., 2024). Though RS-specific CLIP variants aim to reduce the domain gap with aerial and satellite training data (Zhang et al., 2024b; Liu et al., 2024c; Wang et al., 2024d; Ye et al., 2024), they exclusively take RGB as inputs without using multispectral information.

Beyond CLIP-style models, recent RS Vision-Language Models (VLMs) such as RemoteSAM (Yao et al., 2025b), GeoPixel (Shabbir et al., 2025), and Falcon (Yao et al., 2025a) extend language-guided perception to EO via Visual Question Answering (VQA) and referring segmentation tasks. However, their heavy reliance on high-resolution RGB imagery and instance-level semantics constrains their effectiveness for dense LULC segmentation involving region-level classes and multispectral data.

## 3. LAS Dataset

For LULC FM training, we curated the LAS dataset, comprising eight subsets from diverse sources, as shown in Fig. 2. Designed to bridge gaps between natural image processing and LULC mapping, LAS addresses:

- integration of multispectral RS data beyond RGB;
- adaptation to medium-to-low-resolution RS imagery;
- domain knowledge of land surface properties.

As a result, LAS includes ~150k globally distributed sample points (~311k image patches and ~200k label masks) across eight subsets (see Tab. 1):

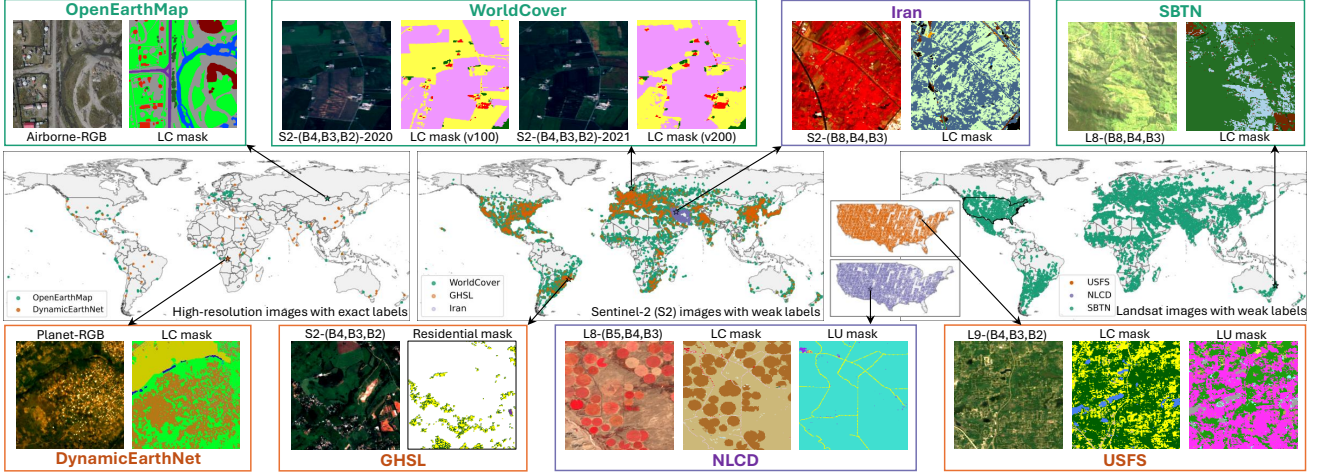


**Fig. 2:** LAS dataset for LandSegmenter training. **Middle:** geographic distributions of each subset. From left to right, read the distributions of high-resolution, Sentinel-2 (S2), and Landsat-8/9 (L8/9) subsets. **Top and Bottom:** examples from each subset. Please refer to Appendix for details including the category information and color systems.

- 1) high-resolution RGB subset from OpenEarthMap (Xia et al., 2023) (GSD: 0.25–0.5m, patch size: 320);
- 2) RGB-NIR subset from DynamicEarthNet (Toker et al., 2022) (GSD: 3–4m; patch size: 256);
- 3) three Sentinel-2 (S2) subsets (GSD: 10m; 12–13 bands; patch size: 264) following the sampling in Wang et al. (2023a);
- 4) three Landsat-8/9 (L8/9) subsets (GSD: 30m; 7–11 bands; patch size: 264) following the sampling in Stewart et al. (2024).

Among them, 1) and 2) are manually annotated, publicly available datasets, while the remaining six pair RS imagery with LULC products downloaded through Google Earth Engine (GEE)<sup>1</sup>, resulting in ~80% weak labels of the whole dataset. This reflects real-world RS data: scarce high-resolution manual annotations versus abundant, imperfect labels often in low resolution. The subsets have varied class systems (coarse to fine, LC and LU categories), with some designed for specific themes (e.g., residential areas). We harmonized these diverse class systems and applied the renaming trick to augment the text corpus (see the Appendix for the full lists of used class name strings).

## 4. LandSegmenter Model

We introduce the architecture of LandSegmenter in Sec. 4.1, followed by its training details in Sec. 4.2.

### 4.1. Architecture

LandSegmenter has three key components: an RS-imagery-adaptive visual encoder, an LULC class name text prompt encoder, and a vision-text collaborative decoder.

**Encoder** LandSegmenter’s encoder adopts SAM2’s Hiera backbone as its core structure in a hierarchical fashion.

<sup>1</sup><https://developers.google.com/earth-engine/datasets/catalog>

Drawing inspiration from Chen et al. (2024b) and Woo et al. (2018), we incorporate an attention-based adapter to enhance multispectral RS image processing. As shown in Fig. 3, AFM is inserted to align the main-stream features and the two specialized components as follows:

- A **High-Frequency (HF) Extractor** that strengthens low-level features and address detail loss;
- The **DOFA Model** (Xiong et al., 2024) that processes multispectral imagery to enrich spectral information.

For HF component extraction, we use the Fast Fourier Transform (fft) and its inverse (ifft) following (Liu et al., 2023). Let  $\mathbf{Z} = \text{fft}(\mathbf{I}^{(c)})$  be the frequency component of the  $c$ th channel of image  $\mathbf{I} \in \mathbb{R}^{H \times W \times C}$ . The HF feature  $\mathbf{I}_{FH}^{(c)}$  is:

$$\mathbf{I}_{FH}^{(c)} = \text{ifft}(\mathbf{Z} \cdot \mathbf{M}(\tau)), \quad (1)$$

where  $\mathbf{M}(\tau)$  is a binary mask eliminating low-frequency coefficients from the image center given the mask ratio  $\tau$ . We apply Eq. (1) to each band and standardize the number of HF component inputs across modalities to six as,

$$\mathbf{I}_{FH} = [\mathbf{I}_{FH}^{(R)}, \mathbf{I}_{FH}^{(G)}, \mathbf{I}_{FH}^{(B)}, \min_c(\mathbf{I}_{FH}^{(c)}), \max_c(\mathbf{I}_{FH}^{(c)}), \overline{\mathbf{I}_{FH}^{(c)}}]. \quad (2)$$

For spectral information extraction, DOFA utilizes a hyper-network to dynamically generate band-specific patch embedding kernels given the central wavelength, leading to modality-tailored features (Xiong et al., 2024). To balance computational efficiency, we adopt DOFA-base to extract the spectral input  $\mathbf{I}_{spe}^b$  for Hiera block  $b = \{1, 2, 3, 4\}$ :

$$\mathbf{I}_{spe}^{(b)} = \text{DOFA}_{l_b}(\mathbf{I}, \mathbf{w}), \quad (3)$$

where  $l_b = \{1, 4, 9, 11\}$  denotes the DOFA output layer indices for Hiera block  $b$ ,  $\mathbf{w}$  is  $\mathbf{I}$ ’s central wavelength vector.

In AFM, we follow Woo et al. (2018) to entangle the three kinds of features with the feature and position attention

**Table 1**

Details of the eight subsets in LAS. Weakly labeled subsets are named after their paired LULC products. A ‘‘point’’ denotes a geospatially unique sampling location. L1C and L2A refer to S2 processing levels, corresponding to Top-of-Atmosphere (TOA) reflectance and Surface Reflectance (SR) images, respectively. ‘‘Res’’ and ‘‘Imp’’ are short for residential and impervious.

Label	Name	#point	Scope	Sensor	GSD	#band	Year	#class	Notes
Exact	Open EarthMap	25.0k	Global	Multiple	0.25-0.5m	3	-	8	Big tiles were cropped to small patches (320x320).
	Dynamic EarthNet	4.8k	Global	Planet	3-4m	4	2018-2019	7	Big tiles were cropped to small patches (256x256). Each point has the data from 4 seasons.
Weak	Iran	5.5k	Iran	S2(L1C)	10-60m	13	2017	10	All bands were upsampled to 10m.
	GHSL	9.3k	Global	S2(L1C)	10-60m	13	2018	Res:3	All bands were upsampled to 10m.
	World Cover v100/200	44.0k	Global	S2(L1C /L2A)	10-60m	12	2020-2021	11	Each point corresponds to two data triples: (L1C, L2A, LC-v100) and (L1C, L2A, LC-v200) from years 2020 and 2021. The L1C-B10 (cirrus) band is discarded to ensure band consistency with L2A.
	NLCD	18.7k	USA	L8 (SR/TOA)	30m	7/11	2019	LC:16 Imp:3	Each point corresponds to a data quadruple: (SR, TOA, LC, Imp).
	USFS	18.7k	USA	L9 (SR/TOA)	30m	7/11	2023	LC:12 LU:5	Each point corresponds to a data quadruple: (SR, TOA, LC, LU).
	SBTN	22.7k	Global	L8 (SR/TOA)	30m	7/11	2020	11	Each point corresponds to a data triple: (SR, TOA, LULC).
<b>Total</b>		148.6k	Global	Multiple	0.25-30m	3-13	-2023	3-16	Images of different processing levels serve as a data augmentation strategy during training.

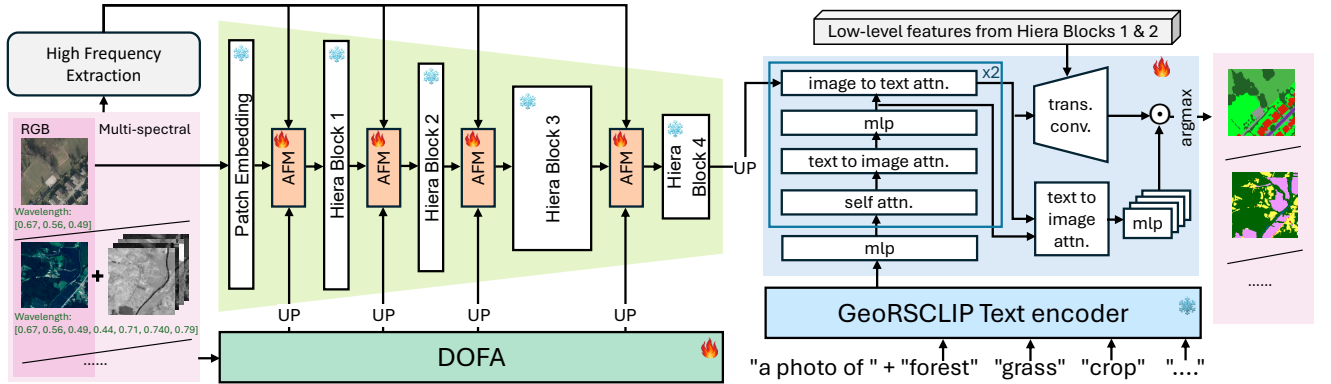


**Fig. 3:** Architecture of LandSegmenter, where the attention-based fusion module (AFM) is depicted per block to indicate the consistent additional input at every stage, with its layer-wise implementation detailed in Fig. 4. The embeddings sent to the decoder are the summation of the outputs from Blocks 4 (upsampled) and 3. For simplicity, we omit this operator in the figure.

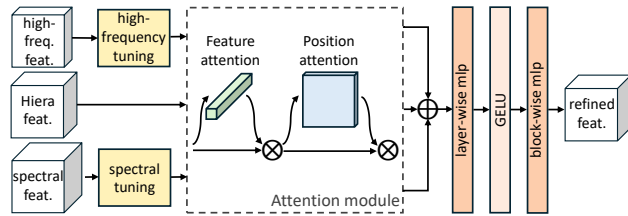


**Fig. 4:** Attention-based fusion module (AFM), where the attention modules share the same architecture yet are individually optimized for each input.

as demonstrated in Fig. 4. Let  $\mathbf{E}_i$  be the Hiera output from the  $i$ th layer. The refined features by AFM are,

$$\mathbf{I}_{ref}^{(b,i)} = \text{MLP}_b(\text{GELU}(\text{MLP}_i(\tilde{\mathbf{E}}_i + \tilde{\mathbf{I}}_{HF} + \tilde{\mathbf{I}}_{spe}^{(b)}))), \quad (4)$$

where  $\text{MLP}_b$  and  $\text{MLP}_i$  are block-wise and layer-wise multi-layer perceptrons,  $\{\tilde{\mathbf{E}}_i, \tilde{\mathbf{I}}_{HF}, \tilde{\mathbf{I}}_{spe}^{(b)}\}$  are attention-enhanced features derived separately from  $\{\mathbf{E}_i, \mathbf{I}_{HF}, \mathbf{I}_{spe}^{(b)}\}$  with the

operation  $\tilde{\mathbf{F}} = \mathbf{F} \otimes a_f(\mathbf{F}) \otimes a_p(\mathbf{F} \otimes a_f(\mathbf{F}))$ , and  $a_f$  and  $a_p$  represent feature and position attention modules, which can be formulated as follows:

$$\begin{aligned} a_f(\mathbf{F}) &= \sigma(\text{MLP}(\mathbf{F}_{AP}^s) + \text{MLP}(\mathbf{F}_{MP}^s)), \\ \tilde{\mathbf{F}}_f &= \mathbf{F} \otimes a_f(\mathbf{F}), \\ a_p(\tilde{\mathbf{F}}_f) &= \text{conv}([\text{max}_c(\tilde{\mathbf{F}}_f); \text{mean}_c(\tilde{\mathbf{F}}_f)]), \end{aligned} \quad (5)$$

where  $\mathbf{F}_{AP}^s, \mathbf{F}_{MP}^s \in \mathbb{R}^{B \times C}$  are the features obtained with spatial average and max pooling from  $\mathbf{F}$ ,  $\sigma$  is the sigmoid function,  $\text{max}_c$  and  $\text{mean}_c$  are operated along the channel dimension ( $\text{dim}=1$ ),  $\otimes$  is the element-wise multiplication, and  $\text{conv}$  is with a kernel size of 7. For  $\mathbf{I}_{FH}$  and  $\mathbf{I}_{spe}^{(b)}$ , a tuning block, comprising three linear layers interleaved with GELU activations, aligns their feature dimensions with  $\mathbf{E}_i$  before input to the attention module.

**Prompter** To enhance semantic awareness for LULC mapping, we replace the original geometric prompter with a text encoder from GeorSCLIP (Zhang et al., 2024b).

GeoRSCLIP was pretrained on a large corpus of RS image-text pairs with geolocation-informed descriptions, making it better-suited for LULC tasks than other vanilla and RS-based CLIP models (see Sec. 6.2.2). We freeze the text encoder due to the relatively limited text corpus compared to the abundance of images in LAS.

**Decoder** The trainable decoder integrates image embeddings with prompt text embeddings to generate final outputs. First, an MLP aligns text embedding dimensions with image features, followed by two cross-attention blocks for information exchange (first text as queries, then image as queries). Enriched image features are upsampled to the target resolution via a two-layer transpose convolutional structure, which incorporates low-level features from Hiera blocks 1 and 2 at each layer. Image-informed text embeddings undergo an additional cross-attention module (text as queries) and MLPs to generate class prediction weights, enabling flexible LULC segmentation across diverse categories.

## 4.2. Training

We employ a combined loss function of CrossEntropy (CE) and Dice (Jadon, 2020) for training. Predictions are generated class-wise before the softmax layer. Thus, we incorporate both multi-class and binary losses in practice:

$$L = \text{CE}(\tilde{\mathbf{Y}}, \mathbf{Y}) + \text{Dice}(\tilde{\mathbf{Y}}, \mathbf{Y}) + \sum_{k=1..K} (\text{BCE}(\tilde{\mathbf{Y}}_k, \mathbf{Y}_k) + \text{BDice}(\tilde{\mathbf{Y}}_k, \mathbf{Y}_k)), \quad (6)$$

where  $\tilde{\mathbf{Y}}$  and  $\mathbf{Y}$  denote predicted and ground-truth (GT) label masks, and  $k$  is the class index.

Taking into consideration the computational cost and pretrained nature of SAM2 and DOFA, we freeze the Hiera backbone and apply a reduced learning rate to DOFA (0.1 of the others) to preserve their foundational capabilities.

The six S2 and L8/9 subsets of the LAS dataset introduce label noise, which can bias the training process. As noted by Liu et al. (2024b), such semantic noise disproportionately affects the deeper, semantically richer layers. To mitigate overfitting to label noise, we employ an auxiliary decoder during training. Specifically, we adopt a Siamese-like architecture in which only the decoder is duplicated. The encoder is shared and processes all input data, while the two decoders are trained in an alternating fashion: the main decoder handles odd-numbered batches (1, 3, ...), and the auxiliary decoder processes even-numbered batches (2, 4, ...). This simple yet effective strategy has been widely used for handling label noise (Ouali et al., 2020). During inference or transfer, only the main decoder is retained.

## 5. Confidence-guided Fusion for Zero-shot Inference

To boost LandSegmenter’s zero-shot performance on unseen classes beyond LAS, we introduce a class-wise

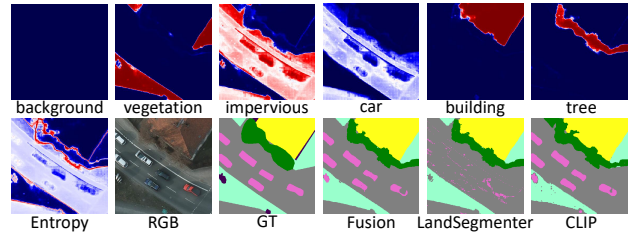


**Fig. 5:** An example from Potsdam where car is absent in the LAS dataset. **Top:** class-wise confidence maps from softmax outputs. **Bottom:** pixel-wise uncertainty map (entropy of probability vectors); RGB image; GT mask; prediction by the confidence-guided fusion strategy (Fusion); prediction by LandSegmenter; prediction by ProxyCLIP with the features refined with LandSegmenter’s embeddings (CLIP). Confidence and uncertainty values range from 0 (blue) to 1 (red). The class scheme of GT and predictions is the same as that in Tab. 3.

confidence-guided fusion strategy (see Fig. 1 (c)). As demonstrated in Fig. 5, we find that LandSegmenter often misclassifies unseen objects (e.g., car as impervious) with low entropy-based uncertainty. At the same time, the class-wise confidence maps for unseen classes remain consistently lower than those for the in-distribution classes of LAS. Motivated by this, we use the maximum confidence score  $C^k = \max(\mathbf{P}^k)$  from each class-wise predicted probability map  $\mathbf{P}^k$  as a fusion indicator: given a predefined confidence threshold  $C_t$ , we treat  $\mathbf{P}^k$  with  $C^k > C_t$  as confident (in-distribution), and those with  $C \leq C_t$  as of low confidence (out-of-distribution or irrelevant classes). In low-confidence cases of LandSegmenter, we prioritize CLIP’s prediction over LandSegmenter’s using a weighted fusion ratio of 3:1 if CLIP shows high certainty. Otherwise, we average predictions from both models with a balanced 2:2 ratio. Formally, let  $\mathbf{P}_{land}^k$  and  $\mathbf{P}_{clip}^k$  denote the predicted probability maps for class  $k$  from LandSegmenter and CLIP, respectively. The fusion process can be formulated as follows,

$$\mathbf{P}_f^k = \begin{cases} 1 \times \mathbf{P}_{land}^k + 3 \times \mathbf{P}_{clip}^k & \text{if } C_{land}^k \leq C_t \text{ and } C_{clip}^k > C_t, \\ 2 \times \mathbf{P}_{land}^k + 2 \times \mathbf{P}_{clip}^k & \text{otherwise.} \end{cases} \quad (7)$$

We further enhance the CLIP-based predictions  $\mathbf{P}_{clip}^k$  by incorporating LandSegmenter’s encoder features via ProxyCLIP (Lan et al., 2024b) before the fusion step. Briefly, ProxyCLIP employs VFM features—here, from LandSegmenter—as queries and keys to compute the attention map, and use the CLIP features as values to produce refined predictions. For simplicity, we use PC to represent ProxyCLIP in the following. As shown at the bottom of Fig. 5, the proposed fusion strategy enables the recovery of unseen classes (e.g., car) from CLIP, while retaining confident predictions from LandSegmenter (e.g., low vegetation at the top).

## 6. Experiments

We trained LandSegmenter on the LAS dataset for 50 epochs using the AdamW optimizer (Loshchilov and Hutter, 2018), with an initial learning rate of  $1e - 4$  decaying

**Table 2**

Zero-shot segmentation performance (mIoU/OA) on six test datasets. The best and second-best results are highlighted in **bold** and underlined.

Dataset	Potsdam	LoveDA	NYC	DW	OSM	MultiSenGe	Average
GSD	0.05m	0.3m	1m	10m	10m	10m	
Image (#band)	RGB (3)	RGB (3)	RGB (3)	S2 (13)	S2 (13)	S2 (10)	
#class	6	7	8	9	13	14	
vanilla CLIP (Radford et al., 2021)	32.21/57.45	27.59/46.63	18.35/34.83	23.99/52.55	10.54/48.18	7.43/50.14	20.02/48.30
MaskCLIP (Zhou et al., 2022)	34.69/55.83	27.80/42.43	19.46/38.55	19.39/43.96	9.56/41.02	9.50/45.84	20.07/44.61
SCLIP (Wang et al., 2024b)	40.06/63.91	33.33/51.24	23.83/43.89	25.91/54.00	11.60/47.41	9.98/56.61	24.12/52.84
ClearCLIP (Lan et al., 2024a)	39.38/63.56	32.79/52.30	23.33/41.94	25.85/54.42	11.90/48.50	9.91/55.55	23.86/52.71
SegEarth-OV (Li et al., 2024)	45.28/68.11	36.91/54.40	25.12/46.35	28.23/55.74	13.49/52.87	12.38/60.47	26.90/56.32
PC (w DINO) (Lan et al., 2024b)	43.08/66.61	26.03/38.25	20.65/36.88	37.50/62.57	22.52/54.97	12.79/64.06	27.61/53.25
PC (w SAM2) (Lan et al., 2024b)	41.90/64.32	25.54/37.70	20.00/34.74	35.76/60.88	20.60/53.66	11.55/62.01	25.55/52.44
RemoteCLIP (Liu et al., 2024c)	21.38/40.24	37.22/56.63	24.05/45.79	23.95/48.92	7.32/29.54	8.53/41.04	20.41/43.69
GeoRSCLIP (Zhang et al., 2024b)	39.78/66.23	31.56/50.03	27.38/48.99	27.58/57.13	12.58/56.15	13.99/59.86	25.48/56.40
SkyCLIP (Wang et al., 2024d)	40.44/67.53	32.14/47.87	23.60/44.91	23.96/51.46	8.65/35.56	9.07/51.29	22.98/49.77
RemoteSAM (Yao et al., 2025b)	<b>64.05/77.02</b>	20.44/39.35	7.82/16.69	6.03/17.61	1.31/2.64	1.77/0.43	16.90/25.62
GeoPixel (Shabbir et al., 2025)	24.19/44.76	19.21/31.75	8.86/19.68	21.05/39.95	12.98/38.72	8.95/3.76	15.87/29.77
PC (w LandSegmenter)	43.65/68.50	27.47/39.81	22.16/39.01	40.00/65.36	24.20/58.02	13.99/ <b>67.21</b>	28.58/56.32
LandSegmenter	41.53/72.21	40.40/58.97	31.44/ <b>53.69</b>	44.08/67.37	29.35/71.93	18.07/62.89	34.15/64.51
Confidence-guided Fusion	49.73/ <u>75.43</u>	<b>40.87/59.15</b>	<b>33.34/53.54</b>	<b>46.06/69.35</b>	<b>30.69/74.03</b>	<b>18.92/66.90</b>	<b>36.60/66.40</b>

to  $1e - 6$  via a cosine scheduler. Inputs were randomly cropped to  $256 \times 256$ , with random flipping and rotation for augmentation, and then resized to the required sizes by Hiera and DOFA. Batch size is set to 12 on each GPU. Training on 4 NVIDIA H100 GPUs took  $\sim 44$  hours. We evaluated LandSegmenter’s performance through zero-shot and fine-tuning experiments on six LULC datasets:

- **Potsdam**<sup>2</sup> is a very-high-resolution dataset of 5cm created for urban semantic segmentation. It includes a training split with 24 big tiles and a validation split with 14 big tiles. We crop them to small patches of  $512 \times 512$ , resulting in 2904 and 1694 training and test patches in our experiments. We utilize RGB images as inputs and generate segmentation maps of 6 classes as in Tab. 3.
- **LoveDA** (Wang et al., 2022a) is constructed with 0.3m RGB images obtained from the GEE platform over three Chinese cities, paired with 7-class label masks as in Fig. 6. We crop the initial  $1024 \times 1024$  tiles to  $512 \times 512$ , leading to 9718 and 6505 for training and testing after removing no-data patches.
- **NYC** (Albrecht et al., 2022) is from the publicly available data for the area of New York City (NYC). We utilize NAIP<sup>3</sup>’s RGB images as inputs. The GT masks are provided by the NYC agencies generated based on the 2017 NYC LiDAR survey and other supplementary information with 8 classes as in Fig. 7. We have 6000 training patches and 4000 test patches of  $256 \times 256$  pixels.
- **DW** (Liu et al., 2025) collects the image-label pairs from the training and test sets of the Google Dynamic World (DW) project (Brown et al., 2022). The input images are Sentinel-2 L1C images fetched according to the date and

coordinates of the label masks. It contains 9 basic LC classes as in Fig. 8. The label masks are not densely annotated, leaving uncertain parts unlabeled. We crop them to  $256 \times 256$ , leading to 14163 for training and 1359 for testing after removing no-data patches.

- **OSM** (Liu et al., 2025) is an extension of DW, with labels from OpenStreetMap (OSM)<sup>4</sup>. The labels are cross-checked with those from DW, plus some manual checks to ensure the quality. The labels are even sparser than those of DW due to the volunteered geographic information nature of OSM. Nevertheless, the class categories are finer with many land use classes as in Fig. 9. We have 4821 training and 1428 testing patches of  $256 \times 256$ .
- **MultiSenGe** (Wenger et al., 2023) is constructed from 14 Sentinel-2 L2A tiles over the GrandEst region in France. The reference data is from the Land Use Land Cover Database (BD0CCE2) provided by French administrators. The dataset is with 10 bands after excluding 2 low-resolution bands (B1, B10). We randomly split 8157 patches of  $256 \times 256$  into 4157 for training and 4000 for testing. As shown in Fig. 10, its 14 classes have many land use ones, making it challenging for LULC mapping.

These datasets were chosen for varying modalities and class definitions, and more importantly, label reliability. The confidence threshold  $C_t$  for confidence-guided fusion is empirically set to 0.6, with its sensitivity analyzed in Sec. 6.3. The name text prompts used in our experiments are listed in the Appendix. For fine-tuning, we use subsets (0.1 and 0.3) of the training set to evaluate LandSegmenter’s transfer learning capability. We set the initial learning rates for SAM2-related models and other comparison methods to  $5e - 4$  and  $1e - 4$ , respectively, with cross-validation. The cosine

<sup>2</sup><https://www.isprs.org/education/benchmarks/UrbanSemLab/>

<sup>3</sup><https://naip-usdaonline.hub.arcgis.com/>

<sup>4</sup><https://www.openstreetmap.org/>

**Table 3**

Class-wise zero-shot results on Potsdam with bg, veg, imp, bd, LandSeg being background, low vegetation, impervious, building, and LandSegmenter.

Potsdam	IoU (%)					
	bg	veg	imp	car	bd	tree
SegEarth-OV	14.07	50.86	59.81	48.37	57.27	41.33
PC (w DINO)	12.23	49.80	59.58	51.29	55.16	30.45
PC (w SAM2)	9.58	47.38	57.01	59.84	50.46	27.10
RemoteCLIP	9.06	6.00	2.35	11.74	69.82	29.34
GeoRSCLIP	3.76	49.24	51.11	19.46	63.52	<b>51.59</b>
SkyCLIP	2.12	50.98	57.39	31.56	59.69	40.88
RemoteSAM	<b>59.85</b>	33.98	<u>68.55</u>	<b>79.68</b>	<b>92.70</b>	<u>49.54</u>
GeoPixel	7.34	29.23	41.73	14.99	47.65	4.20
PC (w LandSeg)	10.41	52.22	62.18	48.28	59.99	28.85
LandSeg	10.18	53.68	63.10	1.23	80.57	40.40
Fusion	11.16	<b>55.46</b>	<b>68.63</b>	39.49	<u>81.14</u>	42.50

scheduler is used in all the cases to adaptively decay the learning rate to  $1e-6$ . The batch size is 15. The total number of fine-tuning epochs is fixed as 30. We use random flipping and rotation with a rate of 0.5 and 0.2 as data augmentation. One NVIDIA H100 GPU is used for fine-tuning.

## 6.1. Main results

### 6.1.1. Zero-shot

We compare LandSegmenter against state-of-the-art OVSS methods and report their mIoU and Overall Accuracy (OA) scores in Tab. 2. Specifically, we evaluate six CLIP-based methods (vanilla CLIP (Radford et al., 2021), MaskCLIP (Zhou et al., 2022), SCLIP (Wang et al., 2024b), ClearCLIP (Lan et al., 2024a), SegEarth (Li et al., 2024), and ProxyCLIP (PC) (Lan et al., 2024b)), three RS-specific CLIP variants (RemoteCLIP (Liu et al., 2024c), GeoRSCLIP (Zhang et al., 2024b), and SkyCLIP (Wang et al., 2024d)), as well as two RS VLMs (RemoteSAM (Yao et al., 2025b) and GeoPixel (Shabbir et al., 2025)). For RS-specific CLIP variants, we follow Li et al. (2024) and apply FeatUp to enhance detail preservation. Note that we use “zero-shot” to refer to applying models to unseen datasets. In this case, models handle both seen and unseen categories during evaluation. This setup reflects real-world LULC scenarios, where datasets often exhibit partial class overlap. As shown in Tab. 2, LandSegmenter outperforms other considered methods, except on the Potsdam dataset with degraded performance on the unseen car class (see Tab. 3). Here, RemoteSAM performs well on the very-high-resolution Potsdam dataset. RemoteSAM’s training data include Potsdam. Its referring-based training paradigm puts more focus on instance-level targets. Thus, RemoteSAM achieves very high accuracy on object-level categories such as car and building, but performs worse on region-level classes such as low vegetation and impervious surfaces. LandSegmenter shows strong performance, especially on the three low-resolution multispectral datasets, which highlights LandSegmenter’s robustness in challenging RS scenarios.

Our fusion strategy further boosts accuracy on out-of-distribution classes, as demonstrated in Tab. 3. Most CLIP-based methods and their training-free variants struggle with low-resolution data. SegEarth-OV and PC attempt to mitigate this with upsamplers and VFM features to improve spatial awareness. However, integrating LandSegmenter’s encoder in PC yields even greater gains, demonstrating the superior feature extraction capabilities of our model.

For qualitative assessment, we present example segmentation maps produced by various methods in Fig. 6–Fig. 10. These visual comparisons highlight the strengths of LandSegmenter, whose LULC maps consistently preserve finer details and exhibit more accurate semantics. The advantages are particularly pronounced on medium-to-low-resolution datasets. In contrast, vanilla CLIP, trained at the image level, captures only coarse semantics with significant spatial detail loss. Other CLIP-based models, especially those incorporating VFM features, partially improve spatial consistency on high-resolution datasets. The three RS-specific CLIP variants, including RemoteCLIP, GeoRSCLIP, and SkyCLIP, also show limited gains, but still underperform the proposed LandSegmenter. RemoteSAM successfully identifies most building areas in Fig. 6, while GeoPixel only detects buildings from the lower part and trees from the upper part. As GeoPixel is designed for referring RS image segmentation, it struggles to segment all objects without detailed location input. All compared models generalize poorly to low-resolution datasets due to the lack of cross-resolution training data. These results further indicate the effectiveness of the proposed method.

### 6.1.2. Fine-tuning

We assess LandSegmenter’s fine-tuning performance under minimal supervision in Tab. 4. In this setting, we compare LandSegmenter with six state-of-the-art RS VFMs, each designed for different input band configurations. Besides, we also consider three SAM2 variants for comparison. LandSegmenter achieves competitive or superior results across all datasets. LandSegmenter’s flexibility enables it to process diverse datasets without band limitations and the need to change the classification header. Other compared methods have more or less restricted applicability. Comparisons of SAM2+HR and SAM2+HR+DOFA\* reveal the advantage of spectral integration for multispectral data. Their instability shows LAS’s essential role in pretraining for robust fine-tuning.

## 6.2. Ablation study

We conduct ablation experiments to examine the impact of weak supervision, architectural components, and training strategies in LandSegmenter construction, with a particular focus on their contributions to zero-shot performance.

### 6.2.1. Role of weak labels

We evaluate the role of weak labels by selectively excluding different data partitions of LAS during LandSegmenter training. As shown in Tab. 5, using the full LAS dataset yields the best balanced performance across

## LandSegmenter

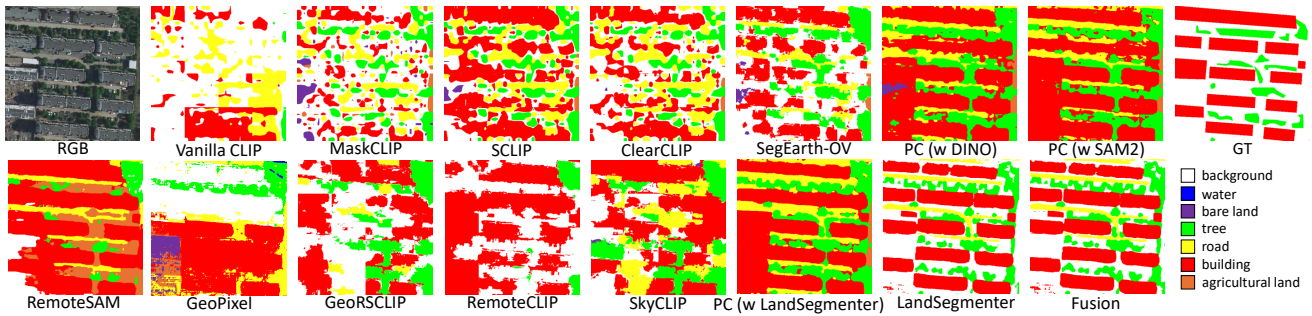


Fig. 6: Segmentation maps generated by various methods on the LoveDA dataset.

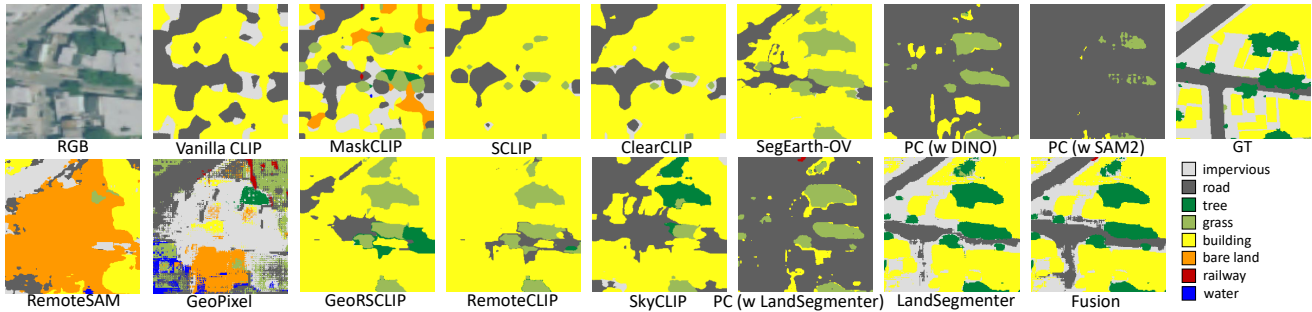


Fig. 7: Segmentation maps generated by various methods on the NYC dataset.

all benchmarks. In LAS, exact (E) and weak (W) label sets correspond to high- and low-resolution imagery, respectively. Excluding either subset degrades performance for the associated resolution, indicating the importance of multi-modal input during training. Notably, removing W leads to substantial performance drops on S2 test sets including DW, OSM, and MultiSenGe, demonstrating the value of weak labels in pretraining. Similarly, excluding the S2-aligned subsets (S) also significantly reduces accuracy on S2 test sets, although the drop is less severe than when both S and Landsat-aligned (L) subsets are excluded. These findings demonstrate the effectiveness and robustness of using weak labels from LULC products for FM training. Interestingly, omitting S has a larger impact on Potsdam, LoveDA, and NYC than excluding L, suggesting stronger interactions and transferability among datasets with similar resolutions. Another key observation is that the confidence-guided fusion

strategy helps mitigate performance gaps caused by partial training data. This finding highlights the effectiveness of the proposed fusion mechanism in enhancing model’s robustness and generalization.

We further provide visual comparisons between LandSegmenter’s predictions and the noisy training labels in Fig. 11. Despite the label noise in the training data, LandSegmenter can avoid overfitting to mislabeled regions and preserve fine spatial details. For example, missing rivers and roads are delineated in the prediction masks. Some mismatches caused by seasonal changes (e.g., wetland to pasture) are also corrected. These results reinforce the effectiveness of these weak labels in large-scale FM training.

### 6.2.2. Architecture design and training strategies

We evaluate the contributions of LandSegmenter’s architectural components in Tab. 6. The full model, combined

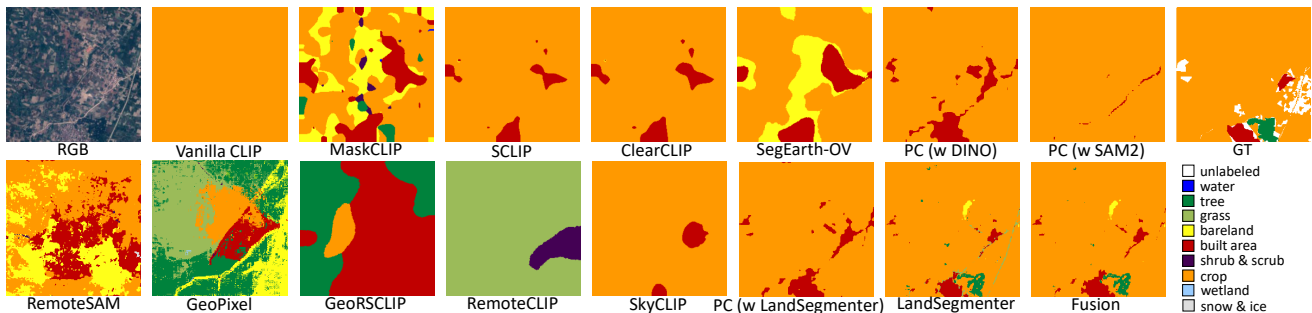


Fig. 8: Segmentation maps generated by various methods on the DW dataset.

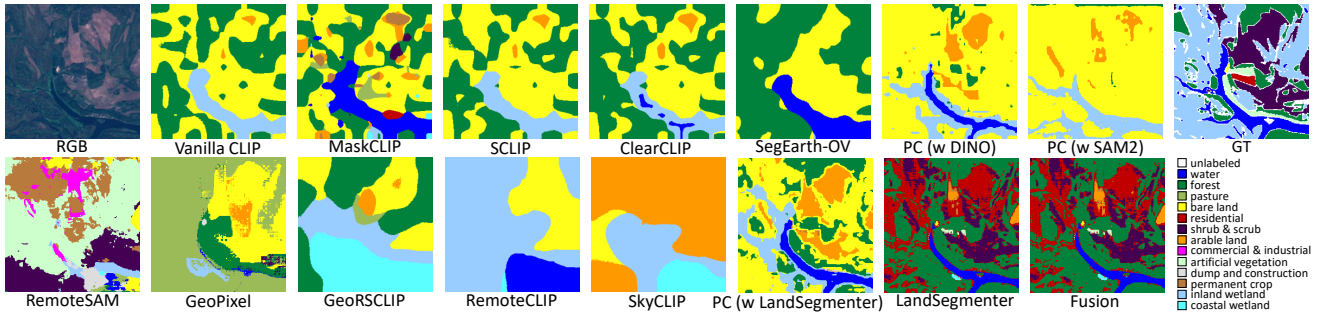


Fig. 9: Segmentation maps generated by various methods on the OSM dataset.

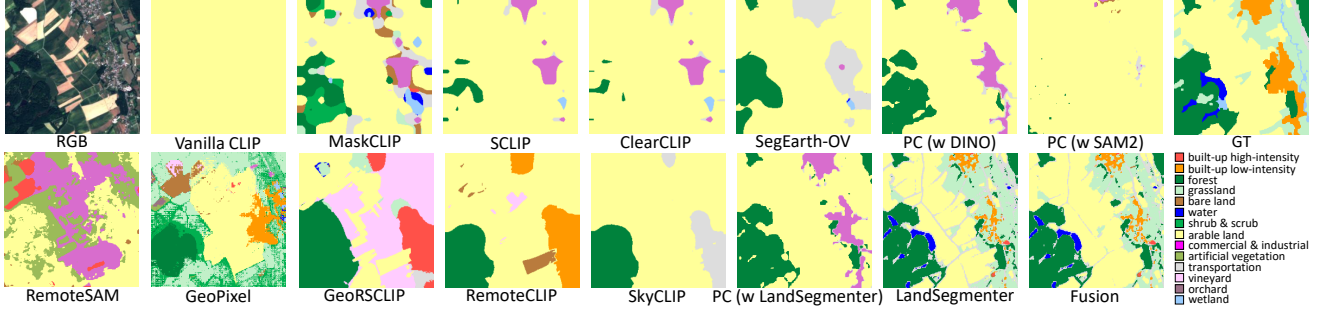


Fig. 10: Segmentation maps generated by various methods on the MultiSenGe dataset.

with our tailored training strategy, achieves the best overall performance. Incorporating the adapter with HR extractors significantly improves results, highlighting both the domain gap of SAM2 on RS imagery and the importance of spatial detail in segmentation tasks. Integrating DOFA to leverage spectral information further boosts accuracy. However, aggressive fine-tuning with a high learning rate can lead to overfitting and reduced generalization. Using fixed DOFA weights without fine-tuning during LandSegmenter training

still yields strong performance, especially when combined with the proposed confidence-guided fusion strategy. This indicates the effectiveness of existing FMs and the benefit of integrating multiple FMs tailored to specific downstream tasks. Moreover, introducing an auxiliary decoder during training leads to consistent gains across the datasets, demonstrating the effectiveness of this simple training technique. Overall, these findings validate the design choices in both the model architecture and training pipeline of LandSegmenter.

Table 4

Fine-tuning results on six test datasets, where DOFA\* refers to the original DOFA weights, while the DOFA models in LandSegmenter are further fine-tuned on the LAS dataset. We utilize UperNet (Xiao et al., 2018) and DeepLabv3+ (Chen et al., 2018) as the segmentation frameworks for ViT-Large (scaleMAE, satMAE, satMAE++, DOFA) and ResNet50 (CromSS, DeCUR) backbones. In SAM2-related models, we fix the backbones (SAM2 and DOFA) during the fine-tuning. For compared methods, all the weights are adjusted. † Failure fine-tuning cases.

Dataset	Potsdam		LoveDA		NYC		DW		OSM		MultiSenGe	
	0.1	0.3	0.1	0.3	0.1	0.3	0.1	0.3	0.1	0.3	0.1	0.3
<b>Training size</b>												
scaleMAE (3B) (Reed et al., 2023)	63.29	67.04	49.46	50.96	<b>56.96</b>	<b>61.88</b>	52.23	55.21	32.20	37.01	36.75	39.82
satMAE (3B) (Cong et al., 2022)	60.31	64.48	47.08	48.85	<u>55.81</u>	<u>61.01</u>	52.90	56.87	34.44	37.76	34.17	37.76
satMAE (10B) (Cong et al., 2022)	-	-	-	-	-	-	46.61	51.44	29.91	33.60	32.35	36.15
satMAE++ (3B) (Noman et al., 2024)	58.47	62.91	44.38	45.77	54.18	59.57	39.70	52.89	22.89	34.44	32.08	34.17
satMAE++ (10B) (Noman et al., 2024)	-	-	-	-	-	-	50.16	54.72	32.26	37.45	33.16	36.17
CromSS (9B) (Liu et al., 2025)	-	-	-	-	-	-	57.89	58.08	36.31	37.33	29.04	36.37
CromSS (13B) (Liu et al., 2025)	-	-	-	-	-	-	59.33	59.38	36.34	42.47	-	-
DeCUR (13B) (Wang et al., 2025)	-	-	-	-	-	-	54.81	55.78	37.50	41.57	-	-
DOFA (Xiong et al., 2024)	61.85	65.97	47.03	48.62	54.29	60.22	54.99	55.66	<u>35.46</u>	39.11	36.76	40.10
SAM2 (3B)	52.27	59.82	42.99	45.24	32.46	43.49	45.82	52.61	24.54	28.80	24.36	29.02
SAM2+HR (3B)	67.09	<u>71.01</u>	47.57	49.83	44.81	53.64	7.88 <sup>†</sup>	60.24	26.07	35.09	33.08	40.58
SAM2+HR+DOFA*	66.59	<u>70.88</u>	47.00	50.16	45.48	57.45	4.07 <sup>†</sup>	<b>61.73</b>	1.62 <sup>†</sup>	35.78	35.41	42.12
<b>LandSegmenter</b>	<b>69.16</b>	<b>71.56</b>	<b>50.74</b>	<b>51.77</b>	54.48	59.41	<b>60.33</b>	<u>60.88</u>	<b>43.46</b>	<b>44.80</b>	<b>41.40</b>	<b>44.75</b>

**Table 5**

Zero-shot segmentation performance (mIoU) by LandSegmenter trained with different data partitions, where **W**, **E**, **S**, and **L** represent the six weak subsets, two exact subsets, three S2 subsets, and three Landsat subsets, respectively.

Method	LandSegmenter					Confidence-guided Fusion					
	Training data	w/o W	w/o E	w/o S	w/o L	Full set	w/o W	w/o E	w/o S	w/o L	Full set
Potsdam	39.57	7.08	41.33	<b>41.65</b>	<u>41.53</u>	41.53	48.43	21.65	47.30	<b>50.66</b>	<u>49.73</u>
LoveDA	<b>41.32</b>	3.43	39.77	40.09	<u>40.40</u>	40.40	<b>41.40</b>	8.76	40.21	40.49	<u>40.87</u>
NYC	25.40	4.38	30.74	<b>31.62</b>	<u>31.44</u>	31.44	32.46	9.28	<u>33.55</u>	<b>35.31</b>	<u>33.34</u>
DW	18.05	<b>44.39</b>	32.54	41.36	<u>44.08</u>	44.08	25.31	<b>46.71</b>	36.96	42.85	<u>46.06</u>
OSM	11.05	<u>28.95</u>	19.45	26.30	<b>29.35</b>	29.35	15.26	30.14	22.54	<u>27.99</u>	<b>30.69</b>
MultiSenGe	9.13	<u>15.36</u>	9.79	<u>15.94</u>	<b>18.07</b>	18.07	12.26	16.34	11.16	<u>17.18</u>	<b>18.92</b>
<b>Average</b>	24.09	17.27	28.94	<u>32.83</u>	<b>34.15</b>	34.15	29.19	22.15	31.95	<u>35.75</u>	<b>36.60</b>

**Table 6**

Zero-shot segmentation performance (mIoU) of the models with different components and training strategies. † Learning rate scale for fine-tuning DOFA.

Method	LandSegmenter							Confidence-guided Fusion									
	HR extractor	DOFA	Auxiliary decoder	✓	✗	0.1†	0†	1†	0.1†	0.1†	✓	✗	0.1†	0†	1†	0.1†	0.1†
Potsdam	✓	✓	✗	✓	✓	✓	✓	✓	✓	✓	✗	1	✗	✓	✓	✓	✓
LoveDA	✗	✗	0.1†	0†	1†	0.1†	0.1†	0.1†	0.1†	0.1†	✗	✗	0.1†	0†	1†	0.1†	0.1†
NYC	✓	✓	✓	✓	✓	✗	✓	✓	✓	✓	✓	✓	✓	✓	✗	✓	✓
Potsdam	26.34	35.05	<u>41.13</u>	37.50	36.97	38.30	<b>41.53</b>	40.76	46.99	48.37	48.51	<b>49.91</b>	48.26	48.26	49.73	<u>49.73</u>	
LoveDA	35.09	40.31	<b>43.11</b>	<u>42.52</u>	39.46	39.47	40.55	37.03	40.37	<b>43.44</b>	<u>43.08</u>	39.61	39.25	40.81	40.81	40.81	
NYC	19.53	15.46	26.76	<u>22.80</u>	14.07	<u>28.76</u>	<b>31.44</b>	21.67	18.65	31.41	<u>25.17</u>	18.07	<b>33.78</b>	33.34	33.34	33.34	
DW	39.26	43.86	41.50	<b>46.65</b>	41.11	43.77	<u>44.08</u>	19.29	36.07	43.78	<b>49.59</b>	44.03	45.40	<u>46.06</u>	46.06	46.06	
OSM	23.11	25.31	25.18	27.92	24.54	<u>28.99</u>	<b>29.35</b>	23.83	16.40	26.44	29.15	25.79	<u>29.81</u>	<b>30.69</b>	30.69	30.69	
MultiSenGe	11.61	15.38	15.57	15.99	16.49	<b>18.65</b>	<u>18.07</u>	12.18	13.22	17.52	17.19	18.53	<b>19.59</b>	18.92	18.92	18.92	
<b>Average</b>	25.82	29.23	32.21	32.23	28.77	<u>32.99</u>	<b>34.17</b>	25.79	28.62	35.16	35.45	32.66	<u>36.02</u>	<b>36.59</b>	36.59	36.59	

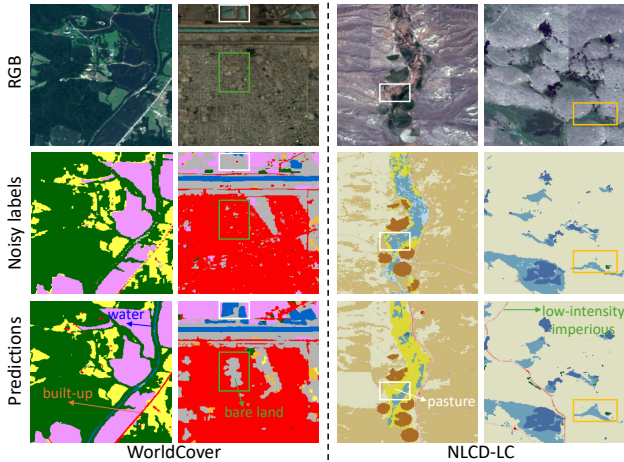


**Fig. 11:** Visual comparison between noisy labels and LandSegmenter predictions from the WorldCover and NLCD-LC training sets. The detailed color scheme is available in the supplementary material.

Then, we evaluate the encoding capability of various CLIP text encoders using Silhouette scores (Rousseeuw, 1987), which measure how well data points (in our case, text embeddings) are clustered based on their semantic similarity. Ranging from -1 to 1, a higher Silhouette score indicates that text embeddings are more tightly grouped within their respective class and well-separated from others, and vice

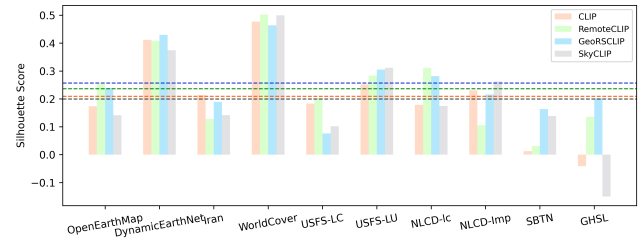


**Fig. 12:** Silhouette scores of text embeddings generated by the text encoders of CLIP, RemoteCLIP, GeoRSCLIP, and SkyCLIP. Dashed lines indicate the mean score values across the datasets. Higher is better.

versa. Specifically, we generate text embeddings for each training set using all augmented text prompts (see Appendix for the full list). We apply t-SNE for dimensionality reduction prior to computing the Silhouette scores. As shown in Fig. 12, the text encoder of GeoRSCLIP achieves the highest scores in most cases, followed by RemoteCLIP, which also demonstrates a strong ability to encode LULC knowledge. SkyCLIP’s text encoder struggles to effectively differentiate among complex LULC classes on some datasets. These findings support our choice of GeoRSCLIP’s text encoder.

### 6.2.3. Region-Level Segmentation Analysis

We evaluate LandSegmenter’s performance on region-level classes (e.g., forest, grass, crop), which dominate

**Table 7**  
Class-wise zero-shot results on the DW dataset.

DW	IoU (%)									mIoU
	water	forest	grass	wetland	crop	shrub	built-up	bare land	ice & snow	
SegEarth-OV	59.12	42.41	2.79	7.98	46.23	0.62	56.46	6.56	31.94	28.23
PC (w DINO)	69.57	55.36	1.78	16.10	65.94	0.77	74.82	15.27	37.88	37.50
PC (w SAM2)	68.77	52.38	0.57	16.39	63.74	0.42	68.65	15.37	35.50	35.76
RemoteCLIP	56.94	23.42	2.59	4.02	40.16	13.26	41.66	10.15	23.37	23.95
GeoRSCLIP	57.29	39.82	5.69	8.50	44.24	3.44	41.41	11.57	36.28	27.58
SkyCLIP	43.58	27.41	0.20	6.85	35.06	0.00	54.65	10.40	37.48	23.96
PC (w LandSegmenter)	72.08	61.16	2.11	22.24	<b>68.65</b>	0.37	<b>78.07</b>	16.26	<b>39.07</b>	40.00
LandSegmenter	82.83	73.98	10.28	34.26	57.54	16.23	66.77	44.40	10.45	44.08
Fusion	<b>83.42</b>	<b>74.58</b>	<b>10.97</b>	<b>35.30</b>	61.80	<b>16.37</b>	71.90	<b>45.00</b>	15.26	<b>46.06</b>



**Fig. 13:** Comparison of forest segmentation by SAM2 (guided by a point prompt, indicated by stars, producing three candidate masks per query) and LandSegmenter (guided by the class name string). Example from the DW dataset.

**Table 8**  
Zero-shot results (mIoU) using the confidence-guided fusion with varying  $C_t$ , where we use abbreviations for Potsdam (Pd), LoveDA (LD), MultiSenGe (MSG), and Average (Avg.).

$C_t$	Pd	LD	NYC	DW	OSM	MSG	Avg.
0.4	46.61	41.00	33.41	46.23	30.62	19.01	36.15
0.5	47.21	40.93	33.37	46.26	30.57	19.00	36.22
0.6	49.73	40.87	33.34	46.06	30.69	18.92	36.60
0.7	49.84	40.83	33.28	45.94	30.24	18.94	36.51
0.8	49.62	40.76	33.25	45.70	30.36	18.87	36.43

LULC mapping but lack clear boundaries. As shown in Fig. 13, LandSegmenter delineates the forest region more accurately than SAM2. This improvement is also reflected in the class-wise results. On the high-resolution Potsdam dataset (see Tab. 3), LandSegmenter achieves higher accuracy on region-level categories such as low vegetation and impervious surfaces. In terms of PC models, replacing SAM2 encoder features with those from LandSegmenter also improves region-level performance. On the low-resolution DW dataset (Tab. 7), where all categories are region-level, the same tendency holds. These results confirm that LandSegmenter enhances regional consistency and segmentation quality in LULC mapping.

### 6.3. Hyperparameter sensitivity

Finally, we investigate the impact of the confidence threshold  $C_t$  on the effectiveness of the fusion strategy. As shown in Tab. 8, the proposed confidence-guided fusion method is robust to variations in this hyperparameter. Nevertheless, a slightly higher threshold above 0.5 tends to yield better performance.

## 7. Conclusions

We propose LandSegmenter, an LULC FM of high input-output flexibility. For its training, we curate the LAS dataset, a large-scale, multi-modal collection predominantly weakly labeled by LULC products, offering a cost-efficient alternative to expensive manual annotations. We also introduce the confidence-guided fusion strategy to boost zero-shot inference. Transfer learning experiments across six diverse LULC datasets demonstrate LandSegmenter's effectiveness, particularly on low-resolution multispectral imagery and zero-shot settings, showing the potential of weak labels in scaling up FM construction. However, this work represents our first step toward building a unified, task-specific LULC FM. Several challenges remain and require further investigation. One notable challenge is the development of more effective strategies to mitigate label noise. Directly integrating advanced learning from noisy labels (LNL) methods into LULC FM training is non-trivial, as most approaches rely on multi-round (Liu et al., 2020), multi-model (Han et al., 2018), or multi-input (Li et al., 2020) learning strategies. Implementing these strategies with pixel-level FMs would significantly increase storage and computational demands due to repeated storage of intermediate results, concurrent training of multiple encoder-decoder models, or processing multiple inputs per iteration. Therefore, lightweight noise-robust strategies are required to enable efficient integration into FM training. Another key challenge is the inherent class imbalance, amplified by the hierarchical nature of LULC classification. While class-wise reweighting according to sample sizes can potentially mitigate this issue, LandSegmenter also need to balance hierarchical semantics and integrate multimodal visual-textual information, making simple data-level adjustments insufficient. Additionally, the current framework employs a fixed text encoder due to the limited text corpus in LAS. Future work will explore fine-tuning strategies to improve its understanding of hierarchical LULC semantics, requiring both specialized data collection and tailored training approaches.

## Acknowledgement

This project is jointly supported by the Munich Center for Machine Learning and the German Research Foundation (DFG GZ: ZH 498/18-1; Project number: 519016653).

## Author Contributions

Chenyang Liu: Conceptualization, Methodology, Experiments, Software, Validation, Formal analysis, Investigation, Data Curation, Visualization, Writing - Original Draft, Review & Editing; Wei Huang: Methodology, Experiments, Formal analysis, Writing - Review & Editing; Xiao Xiang Zhu: Conceptualization, Methodology, Writing - Review & Editing, Project administration, Supervision, Funding acquisition.

## Declaration of generative AI and AI-assisted technologies in the writing process

During the preparation of this work, the authors used ChatGPT in order to improve readability and language. After using this tool/service, the authors reviewed and edited the content as needed and take full responsibility for the content of the publication.

## References

- Albrecht, C.M., Liu, C., Wang, Y., Klein, L., Zhu, X.X., 2022. Monitoring Urban Forests from Auto-Generated Segmentation MAPS, in: IGARSS 2022 - 2022 IEEE International Geoscience and Remote Sensing Symposium, pp. 5977–5980. URL: <https://ieeexplore.ieee.org/document/9884017?arnumber=9884017>, doi:10.1109/IGARSS46834.2022.9884017. iSSN: 2153-7003.
- Astruc, G., Gonthier, N., Mallet, C., Landrieu, L., 2024. OmniSat: Self-Supervised Modality Fusion for Earth Observation. URL: <http://arxiv.org/abs/2404.08351>. arXiv:2404.08351 [cs].
- Brown, C.F., Brumby, S.P., Guzder-Williams, B., Birch, T., Hyde, S.B., Mazzariello, J., Czerwinski, W., Pasquarella, V.J., Haertel, R., Ilyushchenko, S., Schwehr, K., Weisse, M., Stolle, F., Hanson, C., Guinan, O., Moore, R., Tait, A.M., 2022. Dynamic World, Near real-time global 10 m land use land cover mapping. *Scientific Data* 9, 251. URL: <https://www.nature.com/articles/s41597-022-01307-4>, doi:10.1038/s41597-022-01307-4. number: 1.
- Caron, M., Touvron, H., Misra, I., Jégou, H., Mairal, J., Bojanowski, P., Joulin, A., 2021. Emerging Properties in Self-Supervised Vision Transformers, in: ICCV, pp. 9650–9660. URL: [https://openaccess.thecvf.com/content/ICCV2021/html/Caron\\_Emerging\\_Properties\\_in\\_Self-Supervised\\_Vision\\_Transformers\\_ICCV\\_2021\\_paper.html](https://openaccess.thecvf.com/content/ICCV2021/html/Caron_Emerging_Properties_in_Self-Supervised_Vision_Transformers_ICCV_2021_paper.html).
- Chen, K., Liu, C., Chen, H., Zhang, H., Li, W., Zou, Z., Shi, Z., 2024a. RSPrompter: Learning to Prompt for Remote Sensing Instance Segmentation Based on Visual Foundation Model. *IEEE Transactions on Geoscience and Remote Sensing* 62, 1–17. URL: <https://ieeexplore.ieee.org/document/10409216?arnumber=10409216>, doi:10.1109/TGRS.2024.3356074.
- Chen, L.C., Zhu, Y., Papandreou, G., Schroff, F., Adam, H., 2018. Encoder-Decoder with Atrous Separable Convolution for Semantic Image Segmentation, in: ECCV, pp. 801–818. URL: [https://openaccess.thecvf.com/content\\_ECCV\\_2018/html/Liang-Chieh\\_Chen\\_Encoder-Decoder\\_with\\_Atrous\\_ECCV\\_2018\\_paper.html](https://openaccess.thecvf.com/content_ECCV_2018/html/Liang-Chieh_Chen_Encoder-Decoder_with_Atrous_ECCV_2018_paper.html).
- Chen, T., Lu, A., Zhu, L., Ding, C., Yu, C., Ji, D., Li, Z., Sun, L., Mao, P., Zang, Y., 2024b. SAM2-Adapter: Evaluating & Adapting Segment Anything 2 in Downstream Tasks: Camouflage, Shadow, Medical Image Segmentation, and More. URL: <http://arxiv.org/abs/2408.04579>. arXiv:2408.04579 [cs].
- Chen, X., Fan, H., Girshick, R., He, K., 2020. Improved Baselines with Momentum Contrastive Learning. URL: <http://arxiv.org/abs/2003.04297>, doi:10.48550/arXiv.2003.04297. issue: arXiv:2003.04297 arXiv:2003.04297 [cs].
- Chen, Y., Bruzzone, L., 2023. Toward Open-World Semantic Segmentation of Remote Sensing Images, in: IGARSS 2023 - 2023 IEEE International Geoscience and Remote Sensing Symposium, pp. 5045–5048. URL: <https://ieeexplore.ieee.org/document/10281814?arnumber=10281814>, doi:10.1109/IGARSS52108.2023.10281814. iSSN: 2153-7003.
- Chen, Y., Zhang, G., Cui, H., Li, X., Hou, S., Zhu, C., Xie, Z., Li, D., 2025. Superpixel-aware credible dual-expert learning for land cover mapping using historical land cover product. *ISPRS Journal of Photogrammetry and Remote Sensing* 223, 296–316. URL: <https://www.sciencedirect.com/science/article/pii/S0924271625000644>, doi:<https://doi.org/10.1016/j.isprsjprs.2025.02.014>.
- Cong, Y., Khanna, S., Meng, C., Liu, P., Rozi, E., He, Y., Burke, M., Lobell, D., Ermon, S., 2022. SatMAE: Pre-training Transformers for Temporal and Multi-Spectral Satellite Imagery, in: NeurIPS, pp. 197–211. URL: [https://proceedings.neurips.cc/paper\\_files/paper/2022/hash/01c561df365429f33fcd7a7faa4c985-Abstract-Conference.html](https://proceedings.neurips.cc/paper_files/paper/2022/hash/01c561df365429f33fcd7a7faa4c985-Abstract-Conference.html).
- Fuller, A., Millard, K., Green, J., 2023. CROMA: Remote Sensing Representations with Contrastive Radar-Optical Masked Autoencoders, in: NeurIPS. URL: [https://proceedings.neurips.cc/paper\\_files/paper/2023/hash/11822e84689e631615199db3b75cd0e4-Abstract-Conference.html](https://proceedings.neurips.cc/paper_files/paper/2023/hash/11822e84689e631615199db3b75cd0e4-Abstract-Conference.html).
- Ghadiyaram, D., Tran, D., Mahajan, D., 2019. Large-Scale Weakly-Supervised Pre-Training for Video Action Recognition, in: CVPR, pp. 12046–12055. URL: [https://openaccess.thecvf.com/content\\_CVPR\\_2019/html/Ghadiyaram\\_Large-Scale\\_Weakly-Supervised\\_Pre-Training\\_for\\_Video\\_Action\\_Recognition\\_CVPR\\_2019\\_paper.html](https://openaccess.thecvf.com/content_CVPR_2019/html/Ghadiyaram_Large-Scale_Weakly-Supervised_Pre-Training_for_Video_Action_Recognition_CVPR_2019_paper.html).
- Guo, X., Lao, J., Dang, B., Zhang, Y., Yu, L., Ru, L., Zhong, L., Huang, Z., Wu, K., Hu, D., He, H., Wang, J., Chen, J., Yang, M., Zhang, Y., Li, Y., 2023. SkySense: A Multi-Modal Remote Sensing Foundation Model Towards Universal Interpretation for Earth Observation Imagery. URL: <http://arxiv.org/abs/2312.10115>. issue: arXiv:2312.10115 arXiv:2312.10115 [cs].
- Han, B., Yao, Q., Yu, X., Niu, G., Xu, M., Hu, W., Tsang, I.W., Sugiyama, M., 2018. Co-teaching: robust training of deep neural networks with extremely noisy labels, in: Proceedings of the 32nd International Conference on Neural Information Processing Systems, Curran Associates Inc., Red Hook, NY, USA. pp. 8536–8546.
- He, K., Chen, X., Xie, S., Li, Y., Dollár, P., Girshick, R., 2022. Masked Autoencoders Are Scalable Vision Learners, in: CVPR, pp. 16000–16009. URL: [https://openaccess.thecvf.com/content/CVPR2022/html/He\\_Masked\\_Autoencoders\\_Are\\_Scalable\\_Vision\\_Learners\\_CVPR\\_2022\\_paper.html](https://openaccess.thecvf.com/content/CVPR2022/html/He_Masked_Autoencoders_Are_Scalable_Vision_Learners_CVPR_2022_paper.html).
- He, K., Fan, H., Wu, Y., Xie, S., Girshick, R., 2020. Momentum Contrast for Unsupervised Visual Representation Learning, in: CVPR, pp. 9729–9738. URL: [https://openaccess.thecvf.com/content\\_CVPR\\_2020/html/He\\_Momentum\\_Contrast\\_for\\_Unsupervised\\_Visual\\_Representation\\_Learning\\_CVPR\\_2020\\_paper.html](https://openaccess.thecvf.com/content_CVPR_2020/html/He_Momentum_Contrast_for_Unsupervised_Visual_Representation_Learning_CVPR_2020_paper.html).
- He, L., Li, J., Liu, C., Li, S., 2018. Recent Advances on Spectral–Spatial Hyperspectral Image Classification: An Overview and New Guidelines. *IEEE Transactions on Geoscience and Remote Sensing* 56, 1579–1597. URL: <https://ieeexplore.ieee.org/abstract/document/8101519>, doi:10.1109/TGRS.2017.2765364. number: 3.
- Jadon, S., 2020. A survey of loss functions for semantic segmentation, in: 2020 IEEE Conference on Computational Intelligence in Bioinformatics and Computational Biology (CIBCB), pp. 1–7. URL: <https://ieeexplore.ieee.org/document/9277638>, doi:10.1109/CIBCB48159.2020.9277638.
- Ji, W., Li, J., Bi, Q., Liu, T., Li, W., Cheng, L., 2024. Segment Anything Is Not Always Perfect: An Investigation of SAM on Different Real-world Applications. *Machine Intelligence Research* 21, 617–630. URL: <https://doi.org/10.1007/s11633-023-1385-0>, doi:10.1007/s11633-023-1385-0.
- Jia, C., Yang, Y., Xia, Y., Chen, Y.T., Parekh, Z., Pham, H., Le, Q., Sung, Y.H., Li, Z., Duerig, T., 2021. Scaling Up Visual and Vision-Language

- Representation Learning With Noisy Text Supervision, PMLR. pp. 4904–4916. URL: <https://proceedings.mlr.press/v139/jia21b.html>. iSSN: 2640-3498.
- Kaiser, P., Wegner, J.D., Lucchi, A., Jaggi, M., Hofmann, T., Schindler, K., 2017. Learning Aerial Image Segmentation From Online Maps. *IEEE Transactions on Geoscience and Remote Sensing* 55, 6054–6068. doi:10.1109/TGRS.2017.2719738. number: 11.
- Kirillov, A., Mintun, E., Ravi, N., Mao, H., Rolland, C., Gustafson, L., Xiao, T., Whitehead, S., Berg, A.C., Lo, W.Y., Dollár, P., Girshick, R., 2023. Segment Anything. URL: <http://arxiv.org/abs/2304.02643>. arXiv:2304.02643 [cs].
- Lan, M., Chen, C., Ke, Y., Wang, X., Feng, L., Zhang, W., 2024a. ClearCLIP: Decomposing CLIP Representations for Dense Vision-Language Inference, in: Leonardis, A., Ricci, E., Roth, S., Russakovsky, O., Sattler, T., Varol, G. (Eds.), ECCV, Springer Nature Switzerland, Cham. pp. 143–160. URL: [https://link.springer.com/10.1007/978-3-031-72970-6\\_9](https://link.springer.com/10.1007/978-3-031-72970-6_9), doi:10.1007/978-3-031-72970-6\_9. series Title: Lecture Notes in Computer Science.
- Lan, M., Chen, C., Ke, Y., Wang, X., Feng, L., Zhang, W., 2024b. ProxyCLIP: Proxy Attention Improves CLIP for Open-Vocabulary Segmentation, in: Leonardis, A., Ricci, E., Roth, S., Russakovsky, O., Sattler, T., Varol, G. (Eds.), ECCV, Springer Nature Switzerland, Cham. volume 15126, pp. 70–88. URL: [https://link.springer.com/10.1007/978-3-031-73113-6\\_5](https://link.springer.com/10.1007/978-3-031-73113-6_5), doi:10.1007/978-3-031-73113-6\_5. series Title: Lecture Notes in Computer Science.
- Li, C., Hong, D., Zhang, B., Li, Y., Camps-Valls, G., Zhu, X.X., Chanusot, J., 2025a. UrbanSAM: Learning Invariance-Inspired Adapters for Segment Anything Models in Urban Construction. URL: <http://arxiv.org/abs/2502.15199>, doi:10.48550/arXiv.2502.15199. arXiv:2502.15199 [cs].
- Li, J., Socher, R., Hoi, S., 2020. DivideMix: Learning with noisy labels as semi-supervised learning, in: Eighth International Conference on Learning Representations.
- Li, K., Liu, R., Cao, X., Meng, D., Wang, Z., 2024. SegEarth-OV: Towards Training-Free Open-Vocabulary Segmentation for Remote Sensing Images. URL: <http://arxiv.org/abs/2410.01768>. arXiv:2410.01768.
- Li, Y., Wang, H., Duan, Y., Zhang, J., Li, X., 2025b. A closer look at the explainability of Contrastive language-image pre-training. *Pattern Recognition* 162, 111409. URL: <https://www.sciencedirect.com/science/article/pii/S003132032500069X>, doi:10.1016/j.patcog.2025.111409.
- Liu, C., Albrecht, C.M., Wang, Y., Li, Q., Zhu, X.X., 2024a. AIO2: Online Correction of Object Labels for Deep Learning With Incomplete Annotation in Remote Sensing Image Segmentation. *IEEE Transactions on Geoscience and Remote Sensing* 62, 1–17. URL: <https://ieeexplore.ieee.org/document/10460569>, doi:10.1109/TGRS.2024.3373908.
- Liu, C., Albrecht, C.M., Wang, Y., Zhu, X.X., 2024b. Task Specific Pretraining with Noisy Labels for Remote Sensing Image Segmentation, in: IGARSS 2024 - 2024 IEEE International Geoscience and Remote Sensing Symposium, pp. 7040–7044. URL: <https://ieeexplore.ieee.org/abstract/document/10641089>, doi:10.1109/IGARSS53475.2024.10641089. iSSN: 2153-7003.
- Liu, C., Albrecht, C.M., Wang, Y., Zhu, X.X., 2025. Cromss: Cross-modal pretraining with noisy labels for remote sensing image segmentation. *IEEE Transactions on Geoscience and Remote Sensing* 63, 1–17. doi:10.1109/TGRS.2025.3552642.
- Liu, F., Chen, D., Guan, Z., Zhou, X., Zhu, J., Ye, Q., Fu, L., Zhou, J., 2024c. RemoteCLIP: A Vision Language Foundation Model for Remote Sensing. *IEEE Transactions on Geoscience and Remote Sensing* 62, 1–16. URL: <https://ieeexplore.ieee.org/document/10504785?arnumber=10504785>, doi:10.1109/TGRS.2024.3390838.
- Liu, S., Niles-Weed, J., Razavian, N., Fernandez-Granda, C., 2020. Early-Learning Regularization Prevents Memorization of Noisy Labels, in: Advances in Neural Information Processing Systems, Curran Associates, Inc.. pp. 20331–20342. URL: <https://proceedings.neurips.cc/paper/2020/hash/ea89621bee7c88b2c5be6681c8ef4906-Abstract.html>.
- Liu, W., Shen, X., Pun, C.M., Cun, X., 2023. Explicit Visual Prompting for Low-Level Structure Segmentations, in: CVPR, IEEE, Vancouver, BC, Canada. pp. 19434–19445. URL: <https://ieeexplore.ieee.org/document/10203162/>, doi:10.1109/CVPR52729.2023.01862.
- Loshchilov, I., Hutter, F., 2018. Decoupled Weight Decay Regularization. URL: <https://openreview.net/forum?id=Bkg6RiCqY7>.
- Maggiore, E., Tarabalka, Y., Charpiat, G., Alliez, P., 2017. Convolutional Neural Networks for Large-Scale Remote-Sensing Image Classification. *IEEE Transactions on Geoscience and Remote Sensing* 55, 645–657. doi:10.1109/TGRS.2016.2612821. number: 2.
- Mahajan, D., Girshick, R., Ramanathan, V., He, K., Paluri, M., Li, Y., Bharambe, A., van der Maaten, L., 2018. Exploring the Limits of Weakly Supervised Pretraining, in: ECCV, pp. 181–196.
- Noman, M., Naseer, M., Cholakkal, H., Anwer, R.M., Khan, S., Khan, F.S., 2024. Rethinking Transformers Pre-training for Multi-Spectral Satellite Imagery, in: CVPR, pp. 27811–27819. URL: [https://openaccess.thecvf.com/content/CVPR2024/html/Noman\\_Rethinking\\_Transformers\\_Pre-training\\_for\\_Multi-Spectral\\_Satellite\\_Imagery\\_CVPR\\_2024\\_paper.html](https://openaccess.thecvf.com/content/CVPR2024/html/Noman_Rethinking_Transformers_Pre-training_for_Multi-Spectral_Satellite_Imagery_CVPR_2024_paper.html).
- Ouali, Y., Hudelot, C., Tami, M., 2020. Semi-supervised semantic segmentation with cross-consistency training, in: CVPR, pp. 12671–12681. doi:10.1109/CVPR42600.2020.01269.
- Prudente, V.H.R., Skakun, S., Oldoni, L.V., A. M. Xaud, H., Xaud, M.R., Adami, M., Sanches, I.D., 2022. Multisensor approach to land use and land cover mapping in Brazilian Amazon. *ISPRS Journal of Photogrammetry and Remote Sensing* 189, 95–109. URL: <https://linkinghub.elsevier.com/retrieve/pii/S0924271622001289>, doi:10.1016/j.isprsjprs.2022.04.025.
- Radford, A., Kim, J.W., Hallacy, C., Ramesh, A., Goh, G., Agarwal, S., Sastry, G., Askell, A., Mishkin, P., Clark, J., Krueger, G., Sutskever, I., 2021. Learning Transferable Visual Models From Natural Language Supervision, PMLR. pp. 8748–8763. URL: <https://proceedings.mlr.press/v139/radford21a.html>. iSSN: 2640-3498.
- Ravi, N., Gabeur, V., Hu, Y.T., Hu, R., Ryali, C., Ma, T., Khedr, H., Rädle, R., Rolland, C., Gustafson, L., Mintun, E., Pan, J., Alwala, K.V., Carion, N., Wu, C.Y., Girshick, R., Dollár, P., Feichtenhofer, C., 2024. SAM 2: Segment Anything in Images and Videos, in: ICLR. URL: <https://openreview.net/forum?id=Ha6RTeWMD0>.
- Reed, C.J., Gupta, R., Li, S., Brockman, S., Funk, C., Clipp, B., Keutzer, K., Candido, S., Uyttendaele, M., Darrell, T., 2023. Scale-MAE: A Scale-Aware Masked Autoencoder for Multiscale Geospatial Representation Learning, in: ICCV, pp. 4088–4099. URL: [https://openaccess.thecvf.com/content/ICCV2023/html/Reed\\_Scale-MAE\\_A\\_Scale-Aware-Masked-Autoencoder\\_for\\_Multiscale\\_Geospatial\\_Representation\\_Learning\\_ICCV\\_2023\\_paper.html](https://openaccess.thecvf.com/content/ICCV2023/html/Reed_Scale-MAE_A_Scale-Aware-Masked-Autoencoder_for_Multiscale_Geospatial_Representation_Learning_ICCV_2023_paper.html).
- Rousseeuw, P.J., 1987. Silhouettes: A graphical aid to the interpretation and validation of cluster analysis. *Journal of Computational and Applied Mathematics* 20, 53–65. URL: <https://linkinghub.elsevier.com/retrieve/pii/0377042787901257>, doi:10.1016/0377-0427(87)90125-7.
- Shabbir, A., Zumri, M., Bennamoun, M., Khan, F.S., Khan, S., 2025. GeoPixel: Pixel Grounding Large Multimodal Model in Remote Sensing. URL: <http://arxiv.org/abs/2501.13925>, doi:10.48550/arXiv.2501.13925. arXiv:2501.13925 [cs].
- Shan, X., Wu, D., Zhu, G., Shao, Y., Sang, N., Gao, C., 2024. Open-Vocabulary Semantic Segmentation with Image Embedding Balancing, pp. 28412–28421. URL: [https://openaccess.thecvf.com/content/CVPR2024/html/Shan\\_Open-Vocabulary\\_Semantic\\_Segmentation\\_with\\_Image\\_Embedding\\_Balancing\\_CVPR\\_2024\\_paper.html](https://openaccess.thecvf.com/content/CVPR2024/html/Shan_Open-Vocabulary_Semantic_Segmentation_with_Image_Embedding_Balancing_CVPR_2024_paper.html).
- Shankar, S., Stearns, L.A., Veen, C.J.v.d., 2023. Semantic segmentation of glaciological features across multiple remote sensing platforms with the Segment Anything Model (SAM). *Journal of Glaciology*, 1–10. doi:10.1017/jog.2023.95.
- Shi, W., Sui, H., Zhang, C., Zhou, N., Zhou, M., Wang, J., Du, Z., 2025. Efficient metric-resolution land cover mapping using open-access low resolution annotations with prototype learning and modified Segment Anything model. *ISPRS Journal of Photogrammetry and Remote Sensing* 224, 19–41. URL: <https://linkinghub.elsevier.com/retrieve/pii/S0924271625001194>, doi:10.1016/j.isprsjprs.2025.03.021.
- Singh, M., Gustafson, L., Adcock, A., de Freitas Reis, V., Gedik, B., Kosaraju, R.P., Mahajan, D., Girshick, R., Dollár, P., van der Maaten, L., 2022. Revisiting Weakly Supervised Pre-Training of Visual Perception Models, in: CVPR, pp. 804–814. URL: <https://openaccess.thecvf.com/>.

- com/content/CVPR2022/html/Singh\_Revisiting\_Weakly\_Supervised\_Pre-Training\_of\_Visual\_Perception\_Models\_CVPR\_2022\_paper.html.
- Song, H., Kim, M., Park, D., Shin, Y., Lee, J.G., 2021. Learning from Noisy Labels with Deep Neural Networks: A Survey. arXiv:2007.08199 [cs, stat] URL: <http://arxiv.org/abs/2007.08199>. arXiv: 2007.08199.
- Stewart, A.J., Lehmann, N., Corley, I.A., Wang, Y., Chang, Y.C., Braham, N.A.A., Sehgal, S., Robinson, C., Banerjee, A., 2024. SSL4EO-L: Datasets and Foundation Models for Landsat Imagery, in: NeurIPS.
- Sun, X., Wang, P., Lu, W., Zhu, Z., Lu, X., He, Q., Li, J., Rong, X., Yang, Z., Chang, H., He, Q., Yang, G., Wang, R., Lu, J., Fu, K., 2023. RingMo: A Remote Sensing Foundation Model With Masked Image Modeling. IEEE Transactions on Geoscience and Remote Sensing 61, 1–22. URL: <https://ieeexplore.ieee.org/abstract/document/9844015>, doi:10.1109/TGRS.2022.3194732.
- Toker, A., Kondmann, L., Weber, M., Eisenberger, M., Camero, A., Hu, J., Hoderlein, A.P., Senaras, C., Davis, T., Cremers, D., Marchisio, G., Zhu, X.X., Leal-Taixe, L., 2022. DynamicEarthNet: Daily Multi-Spectral Satellite Dataset for Semantic Change Segmentation, in: CVPR, IEEE, New Orleans, LA, USA. pp. 21126–21135. URL: <https://ieeexplore.ieee.org/document/9879359/>, doi:10.1109/CVPR52688.2022.02048.
- Wang, C., Chen, J., Meng, Y., Deng, Y., Li, K., Kong, Y., 2024a. SAMPoly-Build: Adapting the Segment Anything Model for polygonal building extraction. ISPRS Journal of Photogrammetry and Remote Sensing 218, 707–720. URL: <https://linkinghub.elsevier.com/retrieve/pii/S0924271624003563>, doi:10.1016/j.isprsjprs.2024.09.018.
- Wang, F., Mei, J., Yuille, A., 2024b. SCLIP: Rethinking Self-Attention for Dense Vision-Language Inference, in: Leonardis, A., Ricci, E., Roth, S., Russakovsky, O., Sattler, T., Varol, G. (Eds.), ECCV, Springer Nature Switzerland, Cham. pp. 315–332. URL: [https://link.springer.com/10.1007/978-3-031-72664-4\\_18](https://link.springer.com/10.1007/978-3-031-72664-4_18), doi:10.1007/978-3-031-72664-4\_18. series Title: Lecture Notes in Computer Science.
- Wang, J., Zheng, Z., Ma, A., Lu, X., Zhong, Y., 2022a. LoveDA: A Remote Sensing Land-Cover Dataset for Domain Adaptive Semantic Segmentation. URL: <http://arxiv.org/abs/2110.08733>, doi:10.48550/arXiv.2110.08733. arXiv:2110.08733.
- Wang, X., He, W., Xuan, X., Sebastian, C., Ono, J.P., Li, X., Behpour, S., Doan, T., Gou, L., Shen, H.W., Ren, L., 2024c. USE: Universal Segment Embeddings for Open-Vocabulary Image Segmentation, in: CVPR, IEEE, Seattle, WA, USA. pp. 4187–4196. URL: <https://ieeexplore.ieee.org/document/10656965/>, doi:10.1109/CVPR52733.2024.00401.
- Wang, Y., Albrecht, C.M., Braham, N.A.A., Liu, C., Xiong, Z., Zhu, X.X., 2025. Decoupling Common and Unique Representations for Multimodal Self-supervised Learning, in: Leonardis, A., Ricci, E., Roth, S., Russakovsky, O., Sattler, T., Varol, G. (Eds.), ECCV, Springer Nature Switzerland, Cham. pp. 286–303. URL: [https://link.springer.com/10.1007/978-3-031-73397-0\\_17](https://link.springer.com/10.1007/978-3-031-73397-0_17), doi:10.1007/978-3-031-73397-0\_17. series Title: Lecture Notes in Computer Science.
- Wang, Y., Albrecht, C.M., Braham, N.A.A., Mou, L., Zhu, X.X., 2022b. Self-Supervised Learning in Remote Sensing: A review. IEEE Geoscience and Remote Sensing Magazine 10, 213–247. URL: <https://ieeexplore.ieee.org/document/9875399>, doi:10.1109/MGRS.2022.3198244. number: 4.
- Wang, Y., Braham, N.A.A., Xiong, Z., Liu, C., Albrecht, C.M., Zhu, X.X., 2023a. SSL4EO-S12: A large-scale multimodal, multitemporal dataset for self-supervised learning in Earth observation [Software and Data Sets]. IEEE Geoscience and Remote Sensing Magazine 11, 98–106. URL: <https://ieeexplore.ieee.org/abstract/document/10261879>, doi:10.1109/MGRS.2023.3281651. number: 3.
- Wang, Y., Sun, Y., Cao, X., Wang, Y., Zhang, W., Cheng, X., 2023b. A review of regional and Global scale Land Use/Land Cover (LULC) mapping products generated from satellite remote sensing. ISPRS Journal of Photogrammetry and Remote Sensing 206, 311–334. URL: <https://www.sciencedirect.com/science/article/pii/S0924271623003209>, doi:10.1016/j.isprsjprs.2023.11.014.
- Wang, Z., Prabha, R., Huang, T., Wu, J., Rajagopal, R., 2024d. SkyScript: A Large and Semantically Diverse Vision-Language Dataset for Remote Sensing, in: AAAI, pp. 5805–5813. URL: <https://ojs.aaai.org/index.php/AAAI/article/view/28393>, doi:10.1609/aaai.v38i6.28393. number: 6.
- Wenger, R., Puissant, A., Weber, J., Idoumghar, L., Forestier, G., 2023. Multimodal and Multitemporal Land Use/Land Cover Semantic Segmentation on Sentinel-1 and Sentinel-2 Imagery: An Application on a MultiSenGE Dataset. Remote Sensing 15, 151. URL: <https://www.mdpi.com/2072-4292/15/1/151>, doi:10.3390/rs15010151. number: 1.
- Woo, S., Park, J., Lee, J.Y., Kweon, I.S., 2018. CBAM: Convolutional Block Attention Module, in: Ferrari, V., Hebert, M., Sminchisescu, C., Weiss, Y. (Eds.), ECCV, Springer International Publishing, Cham. pp. 3–19. URL: [https://link.springer.com/10.1007/978-3-030-01234-2\\_1](https://link.springer.com/10.1007/978-3-030-01234-2_1), doi:10.1007/978-3-030-01234-2\_1. series Title: Lecture Notes in Computer Science.
- Wu, K., Zhang, Y., Ru, L., Dang, B., Lao, J., Yu, L., Luo, J., Zhu, Z., Sun, Y., Zhang, J., Zhu, Q., Wang, J., Yang, M., Chen, J., Zhang, Y., Li, Y., 2025. A semantic-enhanced multi-modal remote sensing foundation model for Earth observation. Nature Machine Intelligence 7, 1235–1249. URL: <https://www.nature.com/articles/s42256-025-01078-8>, doi:10.1038/s42256-025-01078-8. publisher: Nature Publishing Group.
- Xia, J., Yokoya, N., Adriano, B., Broni-Bediako, C., 2023. OpenEarthMap: A Benchmark Dataset for Global High-Resolution Land Cover Mapping, in: 2023 IEEE/CVF Winter Conference on Applications of Computer Vision (WACV), IEEE, Waikoloa, HI, USA. pp. 6243–6253. URL: <https://ieeexplore.ieee.org/document/10030160/>, doi:10.1109/WACV56688.2023.00619.
- Xiao, T., Liu, Y., Zhou, B., Jiang, Y., Sun, J., 2018. Unified Perceptual Parsing for Scene Understanding, in: ECCV, pp. 418–434. URL: [https://openaccess.thecvf.com/content\\_ECCV\\_2018/html/Tete\\_Xiao\\_Unified\\_Perceptual\\_Parsing\\_ECCV\\_2018\\_paper.html](https://openaccess.thecvf.com/content_ECCV_2018/html/Tete_Xiao_Unified_Perceptual_Parsing_ECCV_2018_paper.html).
- Xiong, Z., Wang, Y., Zhang, F., Stewart, A.J., Hanna, J., Borth, D., Papoutsis, I., Saux, B.L., Camps-Valls, G., Zhu, X.X., 2024. Neural Plasticity-Inspired Multimodal Foundation Model for Earth Observation. URL: <http://arxiv.org/abs/2403.15356>, doi:10.48550/arXiv.2403.15356. arXiv:2403.15356 [cs].
- Yao, K., Xu, N., Yang, R., Xu, Y., Gao, Z., Kitrungratsakul, T., Ren, Y., Zhang, P., Wang, J., Wei, N., Li, C., 2025a. Falcon: A Remote Sensing Vision-Language Foundation Model. URL: <http://arxiv.org/abs/2503.11070>, doi:10.48550/arXiv.2503.11070. arXiv:2503.11070 [cs].
- Yao, L., Liu, F., Chen, D., Zhang, C., Wang, Y., Chen, Z., Xu, W., Di, S., Zheng, Y., 2025b. RemoteSAM: Towards Segment Anything for Earth Observation. URL: <http://arxiv.org/abs/2505.18022>, doi:10.48550/arXiv.2505.18022. arXiv:2505.18022 [cs].
- Ye, C., Zhuge, Y., Zhang, P., 2024. Towards Open-Vocabulary Remote Sensing Image Semantic Segmentation. URL: <http://arxiv.org/abs/2412.19492>, doi:10.48550/arXiv.2412.19492. arXiv:2412.19492 [cs].
- Zhang, C., Bengio, S., Hardt, M., Recht, B., Vinyals, O., 2021. Understanding deep learning (still) requires rethinking generalization. Communications of the ACM 64, 107–115. URL: <https://doi.org/10.1145/3446776>, doi:10.1145/3446776. number: 3.
- Zhang, M., Wang, L., Gu, L., Li, Z., Wang, Y., Ling, T., Tao, X., 2024a. SAM2-PATH: A better segment anything model for semantic segmentation in digital pathology. URL: <http://arxiv.org/abs/2408.03651>. arXiv:2408.03651 [cs, eess].
- Zhang, Z., Zhao, T., Guo, Y., Yin, J., 2024b. RSSM and GeoRSCLIP: A Large-Scale Vision-Language Dataset and a Large Vision-Language Model for Remote Sensing. IEEE Transactions on Geoscience and Remote Sensing 62, 1–23. URL: <https://ieeexplore.ieee.org/document/10679571/?arnumber=10679571>, doi:10.1109/TGRS.2024.3449154.
- Zhao, T., Wang, S., Ouyang, C., Chen, M., Liu, C., Zhang, J., Yu, L., Wang, F., Xie, Y., Li, J., Wang, F., Grunwald, S., Wong, B.M., Zhang, F., Qian, Z., Xu, Y., Yu, C., Han, W., Sun, T., Shao, Z., Qian, T., Chen, Z., Zeng, J., Zhang, H., Letu, H., Zhang, B., Wang, L., Luo, L., Shi, C., Su, H., Zhang, H., Yin, S., Huang, N., Zhao, W., Li, N., Zheng, C., Zhou, Y., Huang, C., Feng, D., Xu, Q., Wu, Y., Hong, D., Wang, Z., Lin, Y., Zhang, T., Kumar, P., Plaza, A., Chanussot, J., Zhang, J., Shi, J., Wang, L., 2024. Artificial intelligence for geoscience: Progress, challenges and perspectives. The Innovation 0. URL: [https://www.cell.com/the-innovation/abstract/S2666-6758\(24\)00129-2](https://www.cell.com/the-innovation/abstract/S2666-6758(24)00129-2), doi:10.1016/j.xinn.2024.100691. publisher: Elsevier.

- Zhou, C., Loy, C.C., Dai, B., 2022. Extract Free Dense Labels from CLIP, in: Avidan, S., Brostow, G., Cissé, M., Farinella, G.M., Hassner, T. (Eds.), ECCV, Springer Nature Switzerland, Cham, pp. 696–712. doi:10.1007/978-3-031-19815-1\_40.
- Zhou, T., Xia, W., Zhang, F., Chang, B., Wang, W., Yuan, Y., Konukoglu, E., Cremers, D., 2024a. Image Segmentation in Foundation Model Era: A Survey. URL: <http://arxiv.org/abs/2408.12957>, doi:10.48550/arXiv.2408.12957. arXiv:2408.12957 [cs].
- Zhou, X., Liang, F., Chen, L., Liu, H., Song, Q., Vivone, G., Chanussot, J., 2024b. MeSAM: Multiscale Enhanced Segment Anything Model for Optical Remote Sensing Images. IEEE Transactions on Geoscience and Remote Sensing 62, 1–15. URL: <https://ieeexplore.ieee.org/document/10522788/?arnumber=10522788>, doi:10.1109/TGRS.2024.3398038.
- Zhu, Q., Lao, J., Ji, D., Luo, J., Wu, K., Zhang, Y., Ru, L., Wang, J., Chen, J., Yang, M., Liu, D., Zhao, F., 2025. Skysense-o: Towards open-world remote sensing interpretation with vision-centric visual-language modeling, in: Proceedings of the Computer Vision and Pattern Recognition Conference (CVPR), pp. 14733–14744.
- Zhu, X.X., Tuia, D., Mou, L., Xia, G.S., Zhang, L., Xu, F., Fraundorfer, F., 2017. Deep Learning in Remote Sensing: A Comprehensive Review and List of Resources. IEEE Geoscience and Remote Sensing Magazine 5, 8–36. URL: <https://ieeexplore.ieee.org/abstract/document/8113128>, doi:10.1109/MGRS.2017.2762307. number: 4.
- Zhu, X.X., Xiong, Z., Wang, Y., Stewart, A.J., Heidler, K., Wang, Y., Yuan, Z., Dujardin, T., Xu, Q., Shi, Y., 2024. On the Foundations of Earth and Climate Foundation Models. URL: <http://arxiv.org/abs/2405.04285>, doi:10.48550/arXiv.2405.04285. arXiv:2405.04285 [cs].

# Appendix of LandSegmenter: Towards a Unified Foundation Model for Land Use and Land Cover Mapping

## A. SLA dataset

### A.1. Class systems and text prompts

Below, we detail the class systems and the corresponding class name text prompts used for training across the eight LAS subsets, as listed in Tabs. A.1 to A.10. With NLCD and USFS each having two layer types, this results in 10 class systems, matched by 10 auxiliary decoders in the SepAux architecture. Each table includes original class names from the LULC products and our reorganized text strings. To standardize class names across subsets, we mainly follow three rules:

- using uniform descriptions for identical definitions (e.g., ‘water’, ‘open water’, and ‘water body’ are unified as ‘water’ and ‘lakes, reservoirs, rivers, and oceans’);
- trying to keep consistent granularity across subsets, using connectors like ‘and’, ‘except for’, and ‘including’ to describe mixed classes (e.g., using ‘except for’ to define the relationship between ‘developed area’ and ‘building’: *developed area except for building*), hoping the model able to learn the simple connections to some extent;
- changing all plural forms to singular for consistency purposes.

**Table A.1**

Class information and corresponding used name texts for the OpenEarthMap (Xia et al., 2023) subset.

Class	Color	Proportion	Original name	Used name text
0	#800000	1.51	Bareland	barren land; bare land; rock, sand, clay and soil
1	#00FF24	22.67	Rangeland	rangeland and herbaceous wetland; grass, pasture, scrub and herbaceous wetland; herbaceous vegetation, shrub and herbaceous wetland; grass, pasture and shrub and herbaceous wetland; herbaceous vegetation, scrub and herbaceous wetland
2	#949494	15.37	Developed space	developed area except for building; built-up area except for building
3	#7030A0	6.62	Road	road; transportation
4	#226126	20.29	Tree	tree and woody wetland
5	#0045FF	3.33	Water	water; lakes, reservoirs, rivers and ocean
6	#4BB549	14.25	Agriculture land	agricultural land; crop; crop land
7	#DE1F07	15.47	Building	building
255	#FFFFFF	0.13	no data	(not used)

**Table A.2**

Class information and corresponding used name texts for the DynamicEarthNet (Toker et al., 2022) subset.

Class	Color	Proportion	Original name	Used name text
0	#949494	7.16	impervious surface	developed impervious area; built-up impervious area
1	#CCCC00	9.55	agriculture	agricultural land; crop; crop land
2	#00FF24	45.49	forest and other vegetation	forest, grass, shrub, pasture and artificial vegetation; tree, herbaceous vegetation and scrub and artificial vegetation; tree, herb, shrub and artificial vegetation; tree, herbaceous vegetation, shrub and artificial vegetation; tree, grass, shrub, pasture and artificial vegetation; forest, herbaceous vegetation, scrub and artificial vegetation; forest, herb, shrub and artificial vegetation
3	#2809C3	0.72	wetland	wetland
4	#B57917	28.06	soil	barren land; bare land; rock, sand, clay and soil
5	#0594C7	8.04	water	water; lakes, reservoirs, rivers and ocean
6	#FFFFFF	0.99	snow and ice	snow and ice

**Table A.3**

Class information and corresponding used name texts for the Iran (Iran Land Cover Map) subset.

Class	Color	Proportion	Original name	Used name text
0	#000000	4.59	Urban	urban area; developed area; residential, commercial, industrial and transportation area; built-up area
1	#006eff	0.58	Water	water; lakes, reservoirs, rivers and ocean
2	#41a661	6.61	Wetland	wetland except for marshland
3	#732600	38.52	Kalut (yardang) Clay Outcrop Uncovered Plain	barren land except for salty land and sand; bare land except for salty land and sand; rock, clay and soil except for salty land
4	#bee8ff	1.58	Marshland	marshland
5	#ff00c5	0.64	Salty Land	salty land
6	#00734c	1.82	Forest	tree; forest; wood; broadleaf and coniferous forest; deciduous and evergreen forest; broadleaf and coniferous tree; deciduous and evergreen tree
7	#d3ffbe	3.17	Sand	sand
8	#446589	30.68	Farm Land	agricultural land; crop; cropland; arable land and permanent crop; herbaceous crop and woody crop; annual crop and orchard and vineyard
9	#cccccc	11.81	Range Land	rangeland; grass, pasture and scrub; herbaceous vegetation and shrub; grass, pasture and shrub; herbaceous vegetation and scrub

**Table A.4**

Class information and corresponding used name texts for the GHSL (Global Human Settlement Layer - Global built-up surface 10m) subset. Unlisted portions denote no data and are masked during training.

Class	Color	Proportion	Original name	Used name text
0	#226126	15.34	open spaces, low vegetation surfaces open spaces, medium vegetation surfaces open spaces, high vegetation surfaces open spaces, water surfaces	non-developed area; non-built-up area; pervious area
1	#FFFF00	13.39	built spaces, residential, building height $\leq 3m$ built spaces, residential, $3m < \text{building height} \leq 6m$ built spaces, residential, $6m < \text{building height} \leq 15m$ built spaces, residential, $15m < \text{building height} \leq 30m$ built spaces, residential, building height $> 30m$	residential area
2	#7030A0	1.11	built spaces, non-residential, building height $\leq 3m$ built spaces, non-residential, $3m < \text{building height} \leq 6m$ built spaces, non-residential, $6m < \text{building height} \leq 15m$ built spaces, non-residential, $15m < \text{building height} \leq 30m$ built spaces, non-residential, building height $> 30m$	non-residential built-up area; non-residential developed area; commercial, industrial and transportation area

**Table A.5**

Class information and corresponding used name texts for the WorldCover (ESA WorldCover 10m v100 and ESA WorldCover 10m v200) subset.

Class	Color	Proportion	Original name	Used name text
0	#006400	21.56	Tree cover	tree including corresponding artificial vegetation and woody crop but except for mangroves; forest including corresponding artificial vegetation and woody crop but except for mangroves; wood including corresponding artificial vegetation and woody crop but except for mangroves
1	#ffbb22	6.75	Shrubland	shrub and scrub including corresponding artificial vegetation and woody crop; shrub including corresponding artificial vegetation and woody crop; scrub including corresponding artificial vegetation and woody crop
2	#ffff4c	20.13	Grassland	grassland and pasture including corresponding artificial vegetation; herb and pasture including corresponding artificial vegetation; herbaceous vegetation and pasture including corresponding artificial vegetation; grassland and meadow including corresponding artificial vegetation; herb and meadow including corresponding artificial vegetation; herbaceous vegetation and meadow including corresponding artificial vegetation
3	#f096ff	24.03	Cropland	agricultural land except for woody crop; crop except for woody crop; cropland except for woody crop; arable land; herbaceous crop; annual crop
4	#fa0000	4.73	Built-up	built-up area without artificial vegetation; man-made structure without artificial vegetation; residential, commercial, industrial and transportation area without artificial vegetation; developed area without artificial vegetation
5	#b4b4b4	11.97	Bare/sparse vegetation	barren land including mine, dump and construction site; bare land including mine, dump and construction site; rock, sand, clay and soil including mine, dump and construction site
6	#f0f0f0	0.0034	Snow and ice	snow and ice
7	#0064c8	10.24	Permanent water bodies	water; lakes, reservoirs, rivers and ocean
8	#0096a0	0.54	Herbaceous wetland	herbaceous wetland; non-forest wetland
9	#00cf75	0.0425	Mangroves	mangroves
10	#fae6a0	0.0047	Moss and lichen	moss and lichen

**Table A.6**

Class information and corresponding used name texts for the NLCD-LC (USGS National Land Cover Database-landcover) subset.

Class	Color	Proportion	Original name	Used name text
0	#466b9f	2.02	Open water	water; lakes, reservoirs, rivers and ocean
1	#d1def8	0.0038	Perennial ice/snow	ice and snow
2	#dec5c5	2.15	Developed, open space	artificial vegetation; non-agricultural vegetation; artificial or non-agricultural vegetation
3	#d99282	1.1	Developed, low intensity	developed low-intensity imperious area; built-up low-intensity imperious area
4	#eb0000	0.54	Developed, medium intensity	developed medium-intensity imperious area; built-up medium-intensity imperious area
5	#ab0000	0.16	Developed high intensity	developed high-intensity imperious area; built-up high-intensity imperious area
6	#b3ac9f	1.12	Barren land (rock/sand/clay)	barren land including mine, dump and construction site; bare land including mine, dump and construction site; rock, sand, clay and soil including mine, dump and construction site
7	#68ab5f	8.37	Deciduous forest	deciduous or broadleaf forest; deciduous or broadleaf tree; deciduous or broadleaf wood
8	#1c5f2c	12.52	Evergreen forest	evergreen or coniferous forest; evergreen or coniferous tree; coniferous or deciduous wood
9	#b5c58f	2.94	Mixed forest	mixed broadleaf and coniferous forest; mixed deciduous and evergreen forest
10	#ccb879	26.6	Shrub/scrub	shrub and scrub; shrub; scrub
11	#dfdfc2	15.95	Grassland/herbaceous	grassland or herbaceous vegetation; grassland or herb; grass or herb
12	#dcd939	5.13	Pasture/hay	pasture or hay; pasture; meadow
13	#ab6c28	16.1	Cultivated crops	agricultural land; crop; cropland; arable land and permanent crop; herbaceous crop and woody crop; annual crop and orchard and vineyard
14	#b8d9eb	3.95	Woody wetlands	woody wetland
15	#6c9fb8	1.36	Emergent herbaceous wetlands	herbaceous wetland; non-forest wetland

**Table A.7**

Class information and corresponding used name texts for the NLCD-Imp (USGS National Land Cover Database-impervious) subset.

Class	Color	Proportion	Original name	Used name text
0	#ffff00	70.18	Primary road. Interstates and other major roads. Pixels were derived from the 2018 NavStreets Street Data. Secondary road. Non-interstate highways. Pixels were derived from the 2018 NavStreets Street Data. Tertiary road. Any two-lane road. Pixels were derived from the 2018 NavStreets Street Data. Thinned road. Small tertiary roads that generally are not paved and have been removed from the landcover but remain as part of the impervious surface product. Pixels were derived from the 2018 NavStreets Street Data.	road; transportation
1	#9f1feb	29.07	Non-road non-energy impervious. Developed areas that are generally not roads or energy production; includes residential/commercial/industrial areas, parks, and golf courses. Microsoft buildings. Buildings not captured in the NLCD impervious process, and not included in the nonroad impervious surface class. Pixels derived from the Microsoft US Building Footprints dataset. LCMAP impervious. Impervious pixels from LCMAP that were used to fill in gaps left when roads were updated from previous versions of NLCD.	non-transportation and non-energy-related impervious area; non-road and non-energy-related impervious area; impervious area except for road and energy-related area
2	#40dfd0	0.75	Wind turbines. Pixels derived from the US Wind Turbine Dataset, accessed on 1/9/2020. Well pads. Pixels derived from the 2019 Oil and Natural Gas Wells dataset from the Oak Ridge National Laboratory. Other energy production. Areas previously identified as well pads and wind turbines and classified in coordination with the Landfire project.	energy-related impervious area

**Table A.8**

Class information and corresponding used name texts for the USFS-LC (USDA Forest Service Landscape Change Monitoring System-Land\_Cover) subset.

Class	Color	Proportion	Original name	Used name text
0	#005e00	34.01	Trees	tree; forest; wood; broadleaf and coniferous forest; deciduous and evergreen forest; broadleaf and coniferous tree; deciduous and evergreen tree
1	#00cc00	0.27	Shrubs & Trees Mix	mixed shrub and tree area; mixed scrub and tree area
2	#b3ff1a	3.74	Grass/Forb/Herb & Trees Mix	mixed grass and tree area; mixed herb and tree area; mixed herbaceous and woody area
3	#99ff99	0.05	Barren & Trees Mix	mixed barren and tree area; mixed barren and woody area
4	#e68a00	4.28	Shrubs	shrub and scrub; shrub; scrub
5	#ffad33	12.98	Grass/Forb/Herb & Shrubs Mix	mixed grass and shrub area; mixed herb and shrub area; mixed grass and scrub area; mixed herb and scrub area
6	#ffe0b3	2.57	Barren & Shrubs Mix	mixed barren and shrub area; mixed barren and scrub area
7	#ffff00	35.89	Grass/Forb/Herb	agricultural land and grassland; agricultural land and herbaceous vegetation; agricultural land and herb; grass or herb
8	#aa7700	0.02	Barren & Grass/Forb/Herb Mix	mixed grass and barren area; mixed herb and barren area
9	#d3bf9b	4.23	Barren or Impervious	barren and impervious area; barren land and impervious area
10	#ffffff	0.0018	Snow or Ice	snow and ice
11	#4780f3	1.95	Water	water; lakes, reservoirs, rivers and ocean

**Table A.9**

Class information and corresponding used name texts for the USFS-LU (USDA Forest Service Landscape Change Monitoring System-Land\_Use) subset.

Class	Color	Proportion	Original name	Used name text
0	#efff6b	16.99	Agriculture	agricultural land; crop; cropland; arable land and permanent crop; herbaceous crop and woody crop; annual crop, orchard and vineyard
1	#ff2ff8	2.89	Developed	developed area; urban area; residential, commercial, industrial and transportation area including artificial vegetation; built-up area
2	#1b9d0c	36.99	Forest	tree and woody wetland; forest and woody wetland; wood and woody wetland; broadleaf and coniferous forest, and woody wetland; deciduous and evergreen forest, and woody wetland; broadleaf and coniferous tree, and woody wetland; deciduous and evergreen tree, and woody wetland
3	#97ffff	0.74	Non-Forest Wetland	herbaceous wetland; non-forest wetland
4	#c2b34a	39.57	Rangeland or Pasture	rangeland; grass, shrub and pasture; herbaceous vegetation and shrub; grass, scrub and meadow; herbaceous vegetation and scrub
255	#a1a1a1	2.81	Other	(not used)

**Table A.10**

Class information and corresponding used name texts for the SBTN (SBTN Natural Lands Map-classification) subset.

Class	Color	Proportion	Original name	Used name text
0	#246E24	18.35	natural forests	tree; forest; wood; broadleaf and coniferous forest; deciduous and evergreen forest; broadleaf and coniferous tree; deciduous and evergreen tree
1	#B9B91E	22.14	natural short vegetation	rangeland; grass, pasture and scrub; herbaceous vegetation and shrub; grass, pasture and shrub; herbaceous vegetation and scrub
2	#006eff	2.04	natural water non-natural water	water; lake, reservoir, river and ocean
3	#06A285	0.01	mangrove	mangroves
4	#FEFECC	13.96	bare non-natural bare	barren land; bare land; rock, sand, clay and soil
5	#ACD1E8	0.02	snow	ice and snow
6	#093D09	2.47	wet natural forests natural peat forests wet non-natural tree cover non-natural peat tree cover	woody wetland
7	#732600	2.54	wet natural short vegetation natural peat short vegetation wet non-natural short vegetation non-natural peat short vegetation	herbaceous wetland; non-forest wetland
8	#D3D3D3	26.43	crop	agricultural land; crop; cropland; arable land and permanent crop; herbaceous crop and woody crop; annual crop, orchard and vineyard
9	#ff7f7f	4.8	built	urban area including mine site, dump site and construction site; developed area including mine site, dump site and construction site; residential, commercial, industrial and transportation area including mine site, dump site and construction site; built-up area including mine site, dump site and construction site
10	#ffaa00	7.04	non-natural tree cover non-natural short vegetation	artificial vegetation

**Table A.11**

Data types and band statistics of LAS subsets. †HR: high-resolution, OEM: OpenEarthMap, DEN: DynamicEarthNet, WC: WorldCover.

subset	dtype	#band	wavelength
HR†	OEM†	uint8	3:RGB
	DEN†	float32	4:RGB-NIR
S2	Iran	uint16	13:[B1,B2,B3,B4,B5,B6,B7,B8, B8A,B9,B10,B11,B12]
	GHSL		[0.443, 0.490, 0.56, 0.665, 0.705, 0.740, 0.783, 0.842, 0.865, 0.940, 1.375, 1.61, 2.19]
	WC†	uint16	12:[B1,B2,B3,B4,B5,B6,B7,B8, B8A,B9,B11,B12]
L8/9	NLCD	TOA:float32 SR:uint16	11(TOA):[B1,B2,B3,B4,B5,B6,B7, B8,B9,B10,B11]
	USFS		TOA:[0.443, 0.482, 0.561, 0.655, 0.865, 1.610, 2.200, 0.590, 1.373, 10.895, 12.005]
	SBTN		7(SR):[B1,B2,B3,B4,B5,B6,B7] SR:[0.443, 0.482, 0.561, 0.655, 0.865, 1.610, 2.200]

**Table A.12**

Band-wise mean and standard deviation (std) values of the images in the LAS subsets. The same abbreviations are applied here as in Tab. A.11.

subset	mean	std
HR	OEM	[123.68, 116.28, 103.53]
	DEN	[58.395, 57.12, 57.375]
S2	Iran	[1042.59, 915.62, 671.26, 2605.21]
	GHSL	[786.79, 850.35, 875.06, 1138.85, 1122.18, 1161.59, 1274.39, 2371.72, 2299.90, 2560.30, 830.07, 22.10, 2177.07, 1524.07]
	WC	L1C:[1605.58, 1390.78, 1314.87, 1363.52, 1549.44, 2091.75, 2371.72, 2299.90, 2560.30, 830.07, 2177.07, 1524.07] L2A:[752.41, 884.30, 1144.16, 1297.47, 1624.91, 2194.64, 2422.21, 2517.76, 2581.65, 2645.52, 2368.51, 1805.07]
L8/9	NLCD	TOA:[0.048360974, 0.054451246, 0.067494757, 0.099091828, 0.098961689, 0.13054624, 0.12400048, 0.077818833, 0.0047299736, 10.850907, 10.487716]
	USFS	SR:[2375.5134, 2545.028, 2975.2673, 4044.3245, 3713.504, 4925.688, 4821.258]
	SBTN	SR:[2375.5134, 2545.028, 2975.2673, 4044.3245, 3713.504, 4925.688, 4821.258]

## A.2. Statistics

Below, we give the central wavelength information serving as the input of DOFA, along with the band-wise mean and standard deviation (std) values used for data normalization for the LAS dataset.

**Table A.13**

Class information of the Potsdam test set. The [first name text prompt](#) is used in fine-tuning experiments.

Class	Color	Original name	Name text prompts for zero-shot inference
0	#440154	background	<a href="#">barren land</a> ; bare land; water; crop; agricultural land; rock, sand, clay and soil; wetland; ice and snow
1	#99FFCC	low vegetation	<a href="#">grass</a> , shrub and scrub; herb; scrub; shrub; grass
2	#808080	impervious surface	<a href="#">road</a> ; transportation; impervious area except for building
3	#E86ACD	car	<a href="#">car</a>
4	#FFFF19	building	<a href="#">building</a>
5	#008000	tree	<a href="#">tree</a> ; forest

**Table A.14**

Class information of the LoveDA (Wang et al., 2022a) test set. The [first name text prompt](#) is used in fine-tuning experiments.

Class	Color	Original name	Name text prompts for zero-shot inference
0	#FFFFFF	background	<a href="#">impervious area except for road and building</a> ; grass; shrub; scrub
1	#FF0000	building	<a href="#">building</a>
2	#FFFF19	road	<a href="#">road</a> ; transportation
3	#0000FF	water	<a href="#">water</a>
4	#7030A0	barren	<a href="#">barren land</a> ; bare land; soil; rock, sand, clay and soil
5	#00FF00	forest	<a href="#">tree</a> ; forest
6	#E97132	agriculture	<a href="#">agricultural land</a> ; crop; crop land

**Table A.15**

Class information of the NYC (New York City) (Albrecht et al., 2022) test set. The [first name text prompt](#) is used in fine-tuning experiments.

Class	Color	Original name	Name text prompts for zero-shot inference
0	#00823C	tree canopy	<a href="#">tree</a>
1	#9BBB59	grass/shrubs	<a href="#">grass</a> ; herb
2	#FF9900	bare soil	<a href="#">bare land</a> ; barren land; rock, sand, clay and soil
3	#0000FF	water	<a href="#">water</a>
4	#FFFF19	buildings	<a href="#">building</a>
5	#5F5F5F	road	<a href="#">road except for railway</a> ; transportation except for railway
6	#DDDDDD	other impervious	<a href="#">impervious area except for road and building</a>
7	#C00000	railroads	<a href="#">railway</a>

## B. Test sets

### B.1. Class systems and text prompts

Below we list the class systems and name strings used for test sets in our experiments.

**Table A.16**

Class information of the DW (Dynamic world) (Liu et al., 2025) test set. The [first name text prompt](#) is used in fine-tuning experiments.

Class	Color	Original name	Name text prompts for zero-shot inference
0	#0000FF	water	<a href="#">water</a>
1	#00823C	trees	<a href="#">tree</a> ; forest; wood
2	#9BBB59	grass	<a href="#">grass</a> ; herb
3	#99CCFF	flooded vegetation	<a href="#">wetland</a>
4	#FF9900	crops	<a href="#">crop</a> ; agricultural land
5	#440154	shrub & scrub	<a href="#">shrub and scrub</a> ; shrub; scrub
6	#C00000	built area	<a href="#">built-up area</a> ; urban area; developed impervious area
7	#FFFF19	bareland	<a href="#">bare land</a> ; barren land; rock, sand, clay and soil
8	#DDDDDD	ice and snow	<a href="#">ice and snow</a>

**Table A.17**

Class information of the OSM (OpenStreetMap) (Liu et al., 2025) test set. The [first name text prompt](#) is used in fine-tuning experiments.

Class	Color	Original name	Name text prompts for zero-shot inference
0	#C00000	Urban fabric	<a href="#">residential area</a>
1	#FF9900	Arable land	<a href="#">arable land</a>
2	#00823C	Forest	<a href="#">forest</a> ; tree
3	#FF00FF	Industrial, commercial & transport	<a href="#">industrial, commercial and transportation area</a>
4	#CCFFCC	Artificial, non-agricultural vegetation	<a href="#">artificial, non-agricultural vegetation</a>
5	#DDDDDD	Mine, dump & construction	<a href="#">mine, dump and construction site</a>
6	#9BBB59	Pastures	<a href="#">pasture</a>
7	#B97B3D	Permanent crops	<a href="#">permanent crop</a>
8	#0000FF	Water bodies	<a href="#">water</a>
9	#FFFF19	Open spaces	<a href="#">bare land</a> ; barren land; rock, sand, clay and soil
10	#440154	Shrub & herbaceous associations	<a href="#">shrub and herbaceous vegetation</a>
11	#99CCFF	Wetlands	<a href="#">inland wetland</a>
12	#5BFFFF	Coastal wetlands	<a href="#">coastal wetland</a>

**Table A.18**

Class information of the MultiSenGe (Wenger et al., 2023) test set. The [first name text prompt](#) is used in fine-tuning experiments.

Class	Color	Original name	Name text prompts for zero-shot inference
0	#FF5149	Dense Built-Up	<a href="#">built-up high-intensity impervious area</a>
1	#FF9900	Sparse Built-Up	<a href="#">built-up low-intensity impervious area</a>
2	#D86DCD	Specialized Built-Up Areas	<a href="#">industrial and commercial area</a>
3	#9BBB59	Specialized but Vegetative Areas	<a href="#">artificial, non-agricultural vegetation</a>
4	#DDDDDD	Large Scale Networks	<a href="#">transportation</a> ; road
5	#FFFF99	Arable Land	<a href="#">arable land</a> ; herbaceous crop
6	#FFCCFF	Vineyards	<a href="#">vineyard</a>
7	#9A7087	Orchard	<a href="#">orchard</a>
8	#C1F0C8	Grasslands	<a href="#">grass</a>
9	#00B050	Groves, Hedges	<a href="#">shrub and scrub</a>
10	#00823C	Forests	<a href="#">forest</a> ; tree
11	#B97B3D	Open Spaces, Mineral	<a href="#">bare land</a> ; barren land; mine site
12	#99CCFF	Wetlands	<a href="#">wetland</a>
13	#0000FF	Water Surfaces	<a href="#">water</a>